Alteration-Induced Volcano Instability at La Soufrière de Guadeloupe (Eastern Caribbean)

Michael J Heap, Tobias S Baumann, Marina Rosas-carbajal, Jean-christophe Komorowski, H. Albert Albert Gilg, Marlène Villeneuve, Roberto Moretti, Patrick Baud, Lucille Carbillet, Claire Harnett, et al.

Alteration-induced volcano instability at La Soufrière de Guadeloupe (Eastern Caribbean)

Michael J. Heap[1,2], Tobias S. Baumann[3,4], Marina Rosas-Carbajal[5], Jean-Christophe Komorowski[5], H. Albert Gilg[6], Marlène Villeneuve[7], Roberto Moretti[5,8], Patrick Baud[1], Lucille Carbillet[1], Claire Harnett[9], and Thierry Reuschlé[1]

[1] Université de Strasbourg, CNRS, Institut Terre et Environnement de Strasbourg, UMR 7063, 5 rue René Descartes, Strasbourg F-67084, France

[2] Institut Universitaire de France (IUF), 1 rue Descartes, Paris 75231, France

[3] Institute of Geosciences, Johannes Gutenberg University Mainz, Germany

[4] Terrestrial Magmatic Systems (TeMaS) Research Platform, Germany

[5] Université de Paris, Institut de Physique du Globe de Paris, CNRS, F-75005 Paris, France

[6] Department of Civil, Geo and Environmental Engineering, Technical University of Munich, Arcisstrasse 21, 80333 Munich, Germany

[7] Department Mineral Resources Engineering, Montanuniversität Leoben, Erzherzog Johann-Straße 3, Leoben A-8700, Austria

[8] Observatoire Volcanologique et Sismologique de Guadeloupe, Institut de Physique du Globe de Paris, F-97113 Gourbeyre, France

[9] School of Earth Sciences, University College Dublin, Dublin, Ireland

*Corresponding author: Michael Heap (heap@unistra.fr; ORCID: 0000-0002-4748-735X)

Abstract

Volcanoes are unstable structures that deform laterally and frequently experience mass wasting events. Hydrothermal alteration is often invoked as a mechanism that contributes

significantly to volcano instability. We present a study that combines laboratory experiments, geophysical data, and large-scale numerical modeling to better understand the influence of alteration on volcano stability, using La Soufrière de Guadeloupe (Eastern Caribbean) as a case study. Laboratory experiments on variably-altered (advanced argillic alteration) blocks show that uniaxial compressive strength, Young's modulus, and cohesion decrease as a function of increasing alteration, but that the internal friction angle does not change systematically. Simplified volcano cross sections were prepared (a homogenous volcano, a volcano containing the alteration zone identified by a recent electrical survey, and a volcano with an artificially enlarged area of alteration) and mechanical properties were assigned to zones corresponding to unaltered and altered rock. Numerical modeling performed on these cross sections, using a hydro-thermo-mechanical modeling code, show (1) the importance of using upscaled values in large-scale models and (2) that alteration significantly increases volcano deformation and collapse volume. Finally, we combined published muon tomography data with our laboratory data to create a 3D strength map, exposing a low-strength zone beneath the southern flank of the volcano coincident with the hydrothermal system. We conclude that hydrothermal alteration decreases volcano stability and thus expedites volcano spreading and increases the likelihood of mass wasting events and associated volcanic hazards. Hydrothermal alteration, and its evolution, should therefore be monitored at active volcanoes worldwide.

Key points

- Laboratory experiments show that hydrothermal alteration reduces the strength of volcanic rock from La Soufrière.

- Numerical modeling shows that hydrothermal alteration significantly increases volcano deformation and collapse volume.

- We provide a 3D strength map of La Soufrière that exposes a low-strength zone coincident with the hydrothermal system.

Plain language summary

The rocks forming a volcanic edifice can be altered by circulating hydrothermal fluids. This alteration can influence the physical and mechanical properties of these rocks, which could jeopardize volcano stability. The stability of a volcanic edifice is an important consideration in volcanic hazards and risk assessments due to the potentially dire consequences of partial volcanic flank collapse. Using a combination of experimental data, geophysical data, and modeling, and La Soufrière de Guadeloupe (Eastern Caribbean, France) as a case study, we find that hydrothermal alteration decreases volcano stability and thus promotes volcano instability and associated volcanic hazards. As a result, we conclude that hydrothermal alteration, and its evolution, should be monitored at active volcanoes worldwide.

Keywords: hydrothermal alteration; uniaxial compressive strength; Young's modulus; upscaling; flank collapse

1 Introduction

Volcanoes are inherently unstable structures that are built haphazardly, in both space and time, from the products of successive effusive and explosive eruptions and endogenous growth. These materials have highly variable physical and mechanical properties (Heap and Violay, 2021) and often form oversteepened and unstable slopes. As a result, volcano deformation (such as volcano spreading; Borgia et al., 2000) and mass wasting events (such as debris avalanches resulting from partial flank collapse, lahars, and rockfalls; Roverato et al., 2021) are commonplace at many volcanoes worldwide. Catastrophic collapse resulting from volcano spreading (van Wyk de Vries and Francis, 1997) and mass wasting events present a significant volcanic hazard, and can also trigger hazardous laterally-directed explosions and devastating—both economically and in terms of loss of life—pyroclastic density currents (Cole et al., 2015; Glicken, 1996; Sparks et al., 2020; Voight et al., 1981). Indeed, partial flank collapses at about 200 volcanoes have resulted in at least 20,000 fatalities in the last 10,000 years (Siebert et al., 2010). Although about 52% of these flank collapses are associated with magmatic eruptions, about 22% are associated with non-magmatic phreatic and/or hydrothermal eruptions (Siebert, 1984; Siebert et al., 1987, 2010). As a result, stability assessments at volcanoes are an essential component of volcano monitoring and volcanic hazard mitigation.

Hydrothermal alteration, common to many volcanoes worldwide, is often invoked as a mechanism that contributes significantly to volcano instability. Indeed, studies using geological evidence, geochemical or geophysical data, numerical modeling, laboratory experiments, or a combination of these approaches have highlighted that hydrothermal alteration has or can weaken a volcanic slope sufficiently to promote collapse (Ball et al., 2013, 2015, 2018; Cecchi et al., 2004; del Potro and Hürlimann, 2009; Finn et al., 2018; John et al., 2008; López and Williams, 1993; Opfergelt et al., 2006; Reid et al., 2001; Rosas-Carbajal et al., 2016; Salaün et

al., 2011; van Wyk de Vries et al., 2000; Voight et al., 2002; Watters et al., 2000). Fluid and pore fluid pressure re-distributions caused by alteration are also thought to promote instability (Ball et al., 2018; Day, 1996; Heap et al., 2021a; Reid, 2004) and erratic explosive behavior (de Moor et al., 2019; Heap et al., 2019; Mick et al., 2021).

Geological evidence is provided by the abundance of hydrothermally altered materials typically found in debris avalanche deposits resulting from partial flank collapse. For example, in their analysis of the 26 December 1997 partial edifice collapse at Soufrière Hills volcano (Montserrat, Eastern Caribbean), Voight et al. (2002) found varicolored, hydrothermally-altered materials within the avalanche deposits, highlighting that alteration could have contributed to the collapse of the southern sector of the volcano. Avalanche deposits and material ejected during phreatic explosions at La Soufrière de Guadeloupe (Eastern Caribbean; France) were also found to contain various parts of the active and ancient hydrothermal systems of the volcano (Salaün et al., 2011). Debris avalanche deposits at Tutupaca volcano (Peru) also contain hydrothermally altered materials (Samaniego et al., 2015). Extensive fumarole activity and hydrothermal alteration on the unstable flanks of Casita volcano (Nicaragua) was documented by van Wyk de Vries et al. (2000), a volcano that experienced a partial flank collapse in 1998 with associated debris avalanches that killed about 2,500 people (Kerle and van Wyk de Vries, 2001; van Wyk de Vries et al., 2000). Opfergelt et al. (2006) further suggested that the presence of abundant smectite (up to 50 wt.%) in the hydrothermally-altered core of Casita volcano contributed to slope instability by acting as a barrier to water infiltration thereby promoting fluid circulation along marked discontinuities, gradually decreasing the shear strength of the host-rock. Finally, more than 55 debris flows have originated from Mt Rainer (USA) in the Holocene, and hydrothermally derived clays have been found in some of the most widespread lahar deposits (Reid et al., 2001).

Geophysical and geochemical evidence has been provided by a wide range of different techniques. For example, electrical tomography data exposed the extent of the hydrothermally altered zone, the location and geometry of low-strength detachment planes, and potential collapse volumes at La Soufrière de Guadeloupe (Rosas-Carbajal et al., 2016). Hyperspectral remote sensing (Kereszturi et al., 2021) and helicopter electromagnetic and magnetic measurements (Finn et al., 2018) have been used to map hydrothermal alteration zones to inform slope stability modeling at Mt Ruapehu (New Zealand) and Mount Baker (USA), respectively, highlighting the most likely location of future collapses. Finally, geochemical data and modeling provided by López and Williams (1993) suggested that hydrothermal alteration along faults can create weak sliding planes that can facilitate slope failure.

Numerical and analog modeling has also provided key insights into how hydrothermal alteration can influence volcano stability. For example, using analogue experiments in which sand-plaster mixtures and silicone were used to represent fresh and altered rock, respectively, van Wyk de Vries et al. (2000) showed that a weak and ductile (hydrothermally altered) core can reproduce the deformation structures observed at Casita volcano, suggesting that hydrothermal alteration destabilized the volcano. Motivated by intensive alteration on the flanks and summit of Mt Rainer, Reid et al. (2001) examined the influence of alteration on volcano stability using a geotechnical method of 3D column limit-equilibrium slope stability analysis. Using a best-estimate distribution of the alteration, and typical values of cohesion, internal friction angle, and rock unit weight for fresh, lightly altered, and highly altered rocks, Reid et al. (2001) concluded that steep slopes and large volumes of altered and weak rock can promote potentially large gravitational failures.

Although these aforementioned studies, and others, have improved our understanding of alteration-induced volcano instability, the shape and size of the alteration zones and/or the geomechanical properties used in large-scale stability modeling are often poorly constrained or

arbitrarily chosen. Indeed, there is a paucity of mechanical data for variably altered volcanic rocks for use in large-scale numerical models designed to better understand flank stability. As noted by Ball et al. (2018), the scarcity of rock physical and mechanical properties for altered volcanic rocks limits the investigation of volcano stability using large-scale models. We present here a multidisciplinary study in which we first provide physical and mechanical properties for variably altered andesites from La Soufrière de Guadeloupe. We then assign laboratory-scale and upscaled (i.e. modified to account for large-scale discontinuities that are not captured in laboratory-scale samples) physical and mechanical properties to zones identified by a recent electrical survey of the dome of La Soufrière de Guadeloupe (Rosas-Carbajal et al., 2016) and perform large-scale numerical modeling to showcase the importance of hydrothermal alteration on volcano stability. Finally, we combine recent muon tomography data (Rosas-Carbajal et al., 2017) with our laboratory data to create a 3D compressive strength map of the volcano. Although we use La Soufrière de Guadeloupe as a case study, we consider our salient conclusions relevant for andesitic stratovolcanoes worldwide.

2 La Soufrière de Guadeloupe (Eastern Caribbean, France)

La Soufrière de Guadeloupe (Figure 1a), henceforth called La Soufrière, is located on the island of Guadeloupe in the Eastern Caribbean (Figure 1b) and is an archetype of the hazardous andesitic volcanoes that occur in many subduction zones. The current lava dome formed in 1530 CE and, since 1635 CE, there have been six non-magmatic phreatic or hydrothermal eruptions (Komorowski et al., 2005). The largest and most-recent eruption occurred in 1976–1977. After months of seismic unrest, the volcano exploded suddenly and without precursory signs in 1976–1977, resulting in a volcanic crisis that led to the evacuation of about 70,000 people and serious socioeconomic consequences for the island (Feuillard et al., 1983; Hincks et al., 2014; Komorowski et al., 2005, 2015).

Volcanic unrest has been increasing since the volcano reawakened in 1992, marked by the restart of fumarolic and seismic activity (Komorowski et al., 2005) and, in April 2018, the largest felt volcano-tectonic earthquake since the 1976–1977 crisis (M_L 4.1 or M_W 3.7; Moretti et al., 2020). The 2018 episode of accelerated unrest was interpreted as a failed phreatic eruption and raised serious concerns for the stability of the southwest flank of the dome, which shows the largest displacements (up to 9 mm/year towards the southwest) over the last 20 years (Moretti et al., 2020). The main features of the ongoing unrest include the continuous expansion of the outgassing area on top of the lava dome and the appearance of new steam-dominated fumaroles in July 2014 and February 2016 that are characterized by a deep magmatic gas component (Brombach et al., 2000; Moretti et al., 2020; Villemant et al., 2014). Such expansion was accompanied by an increase in the heat output from the entire dome, which evolved from ~1.2 MW in 2010 to ~7.6 MW in 2020 (Jessop et al., 2021). This increase in heat output is of great concern for La Soufrière as it has been recently demonstrated that volcanoes with a high heat flux are more likely to experience magmatic or phreatic eruptions (Girona et al., 2021). High-flow rate thermal acid sulfate-chloride springs, associated with degassing of the underlying magmatic body, are observed on the slopes and at the base of the dome and supply hot acid fluids and CO_2, but also SO_2, H_2S, HCl, and HF, to the above hydrothermal system (Villemant et al., 2005; 2014). These acidic fluids are (1) transferred through the dome and feed the steam-rich summit fumaroles and (2) circulate through the dome structure along listric, concave-upward structural discontinuities that drain to the southwest (Brombach et al., 2000; Rosas-Carbajal et al., 2016; Salaün et al., 2011; Villemant et al., 2014). Evidence for the preferential circulation of acidic thermal fluids along these structures is provided by the 3D geometry of thermal springs (Moretti et al., 2020; Villemant et al., 2005) and geophysical imaging (Bouligand et al., 2016; Brothelande et al., 2014; Nicollin et al., 2006; Rosas-Carbajal et al., 2016). The shallow hydrothermal system is considered responsible for the recent

observed shallow deformation and seismic activity (at depths at or above sea level, with magnitudes less than one) (Moretti et al., 2020). Indeed, the monthly bulletins from the observatory (Observatoire Volcanologique et Sismologique de Guadeloupe, Institut de Physique du Globe de Paris (OVSG-IPGP), 1999-2021; available at http://www.ipgp.fr/fr/ovsg/bulletins-mensuels-de-lovsg) document hundreds of shallow, low-magnitude ($M < 1$) earthquakes each month. Deeper and higher magnitude off-axis seismic activity are thought to be related to increases in pore pressure in response to the pulsatory arrival of hot magmatic fluids along the larger faults that cut the dome (Moretti et al., 2020).

The recent unrest, suggesting that La Soufrière is undergoing a renewed period of structural and chemical weakening, raises concern for the stability of the volcano. Indeed, the most-recent unrest and instability at La Soufrière was associated with hydrothermal activity. For example, the materials ejected during the explosive hydrothermal eruption of 1976–1977 were largely hydrothermally altered (Feuillard et al., 1983) and geological studies have also shown that La Soufrière has an exceptional record of partial edifice collapse (at least eight collapses in the past 9,150 years) that have produced extensive debris avalanche deposits dominantly composed of hydrothermally altered materials (Boudon et al., 1987; Komorowski et al., 2005; Le Friant et al., 2006; Peruzzetto et al., 2019; Rosas-Carbajal et al., 2016; Salaün et al., 2011). The simulations of Le Friant et al. (2006) and Peruzzetto et al. (2019) suggest that the northern and eastern parts of the town of Saint Claude could be impacted by small-volume partial dome collapses and that, in the worst-case scenario of a major dome collapse, a large part of Basse-Terre could be affected. As a result, not only is La Soufrière an ideal natural laboratory to study the influence of hydrothermal alteration on volcano stability, but such a study is also timely because of the ongoing, and increasing, unrest at the volcano.

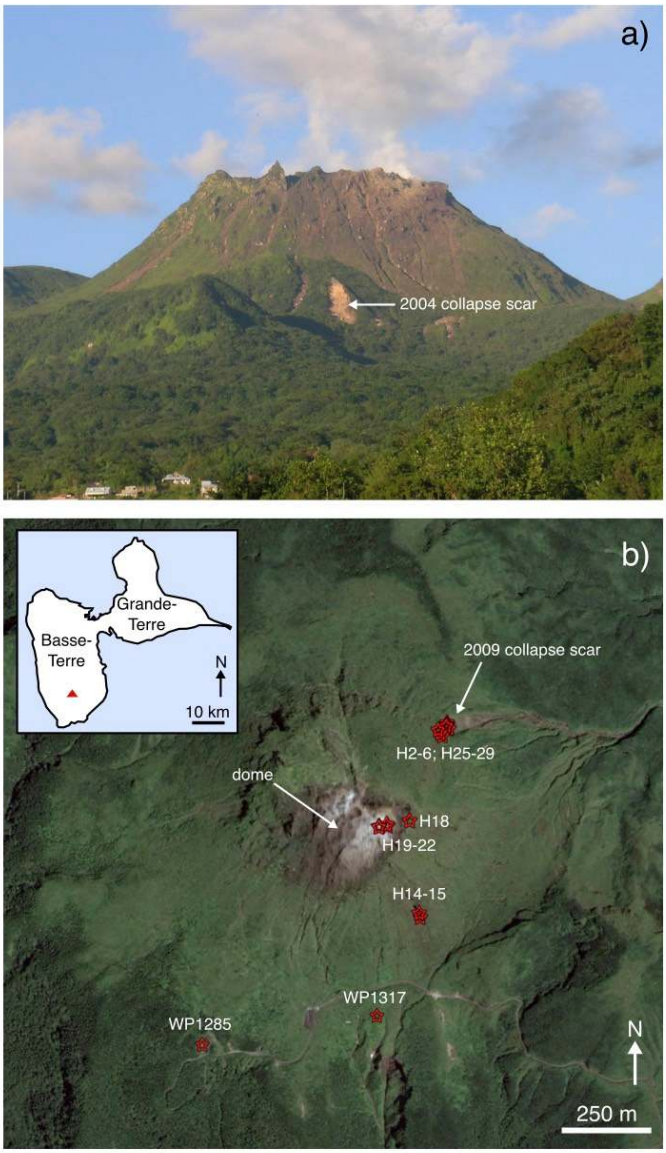

Figure 1. (a) Photograph of La Soufrière de Guadeloupe (Eastern Caribbean, France). This photograph also shows the collapse scar (indicated by the white arrow) triggered by the 21 November 2004 Les Saintes magnitude Mw 6.3 regional earthquake (Feuillet et al., 2011). (b) Map of La Soufrière de Guadeloupe (taken from Google Maps®) showing the sampling locations for the 17 blocks acquired for this study. This image also shows the location of the dome and the 2009 collapse scar (indicated by white arrows). Inset shows a map of Guadeloupe in which the location of La Soufrière de Guadeloupe is indicated by a red triangle.

3 Materials and Methods

A total of 17 blocks were collected from La Soufrière during a field campaign in 2019 (sampling locations shown as red stars in Figure 1b). Our aim was to sample a range of materials from different locations on the volcano that best represent the variability in porosity and hydrothermal alteration of the rocks forming the edifice. A large proportion of the blocks (eight out of 17) were collected from the collapse scar of the 19 November 2009 landslide, triggered by extreme rainfall (Moretti et al., 2020; Peruzzetto et al., 2019), which was seen as an opportunity to sample blocks that are more representative of the interior of the volcano.

Eight blocks were taken from the collapse scar of the 2009 landslide (H2A, H2B, H3, H4A, H5A, H6, H25, and H29), one block was taken from the collapse scar of the landslide triggered by the 21 November 2004 *Les Saintes* magnitude Mw 6.3 regional earthquake (Feuillet et al., 2011; Figure 1b) (WP1285), two blocks were taken from the West wall of the fault "*Faille 30 août*" (H14 and H15), and one block, a volcanic bomb from the 1976–1977 eruption, was taken from the roof of a small disused thermal bathhouse to the South of the dome (WP1317). The remaining samples were taken from the dome: one block was taken from the "*Lacroix Supérieur*" outgassing fracture (H18), and four blocks were taken from the lava spines of the 1530 CE dome: two blocks from "*Cratère Sud Central*" (H19 and H20) and two blocks from an adjacent site (H21 and H22). Site descriptions and Global Positioning System (GPS) coordinates are available for each block in the Supplementary Information.

Cylindrical samples were prepared from each of the blocks to a diameter of 20 mm and then cut and precision-ground to a nominal length of 40 mm. The samples were washed and then dried in a vacuum-oven at 40 °C for at least 48 h. The connected porosity of each sample was calculated using the bulk sample volume and the skeletal (solid) sample volume measured by a helium pycnometer. Dry and wet bulk sample densities were calculated using the bulk sample volume and the dry and wet mass, respectively. Polished thin sections were prepared

from offcuts of the samples for microstructural analysis, performed using a Tescan Vega 2 XMU scanning electron microscope (SEM). The mineral content of the 17 blocks was analyzed and quantified using X-ray powder diffraction (XRPD) on powdered offcuts of the samples, assisted by Raman spectroscopy on the prepared thin sections (see Supplementary Information for more details).

Dry uniaxial compressive strength was measured on oven-dry samples from all 17 blocks in a uniaxial load frame. Samples were deformed under ambient laboratory pressure and temperature at a constant axial strain rate of 10^{-5} s^{-1} until macroscopic failure. The static Young's modulus was determined from the elastic portion of the uniaxial stress-strain curves (Heap et al., 2020a). Triaxial compression experiments were performed on blocks selected to best represent the variability in observed alteration (samples H2B, H3, and H18). These samples were vacuum-saturated in deionized water, inserted into a rubber jacket, placed inside a pressure vessel, and then taken to the target confining (from 10.5 to 25 MPa) and pore fluid pressures (10 MPa for all experiments) using servo-controlled pumps. Samples were deformed under ambient laboratory temperature at a constant axial strain rate of 10^{-5} s^{-1} until either macroscopic failure (for brittle experiments) or until 3% axial strain (for ductile experiments). The triaxial apparatus was also used to measure the water-saturated uniaxial compressive strength of samples H2B, H3, and H18. For both uniaxial and triaxial experiments, axial displacement and axial load were measured using a linear variable differential transducer and a load cell, respectively. Axial displacement (minus the displacement accumulated within the load chain) and axial load were converted to axial strain and axial stress using the sample dimensions. Here, we define the effective pressure, P_{eff}, as the confining pressure, P_c, minus the pore fluid pressure, P_p. We adopt the convention that compressive stresses and strains are positive.

4 Results

4.1 Microstructure, mineralogy, and alteration

The mineral contents for each of the 17 blocks are given in Table 1, and Figure 2 shows backscattered SEM images of three blocks selected to represent the range of alteration intensity (defined by their percentage of secondary minerals) observed in the rocks collected for this study (relatively unaltered – H18; moderately altered – H3; and highly altered – H2B). SEM images of all the blocks are available in the Supplementary Information. All of the andesite blocks are characterized by a porphyritic texture comprising phenocrysts of dominantly plagioclase and pyroxene (and high-density oxides) within a crystallized groundmass (Figure 2). All of the samples also contain secondary minerals, including silica polymorphs (quartz, cristobalite, tridymite, and opal-A), hematite, pyrite, alunite or natroalunite, gypsum, kaolinite, and talc (Table 1). Plagioclase phenocrysts are often pervasively altered and partially replaced by kaolinite (e.g., Figure 2c) or opal-A. Secondary minerals (natroalunite, alunite, cristobalite, tridymite, pyrite, and kaolinite) are also found precipitated within pores and microcracks (see Supplementary Information for additional SEM images).

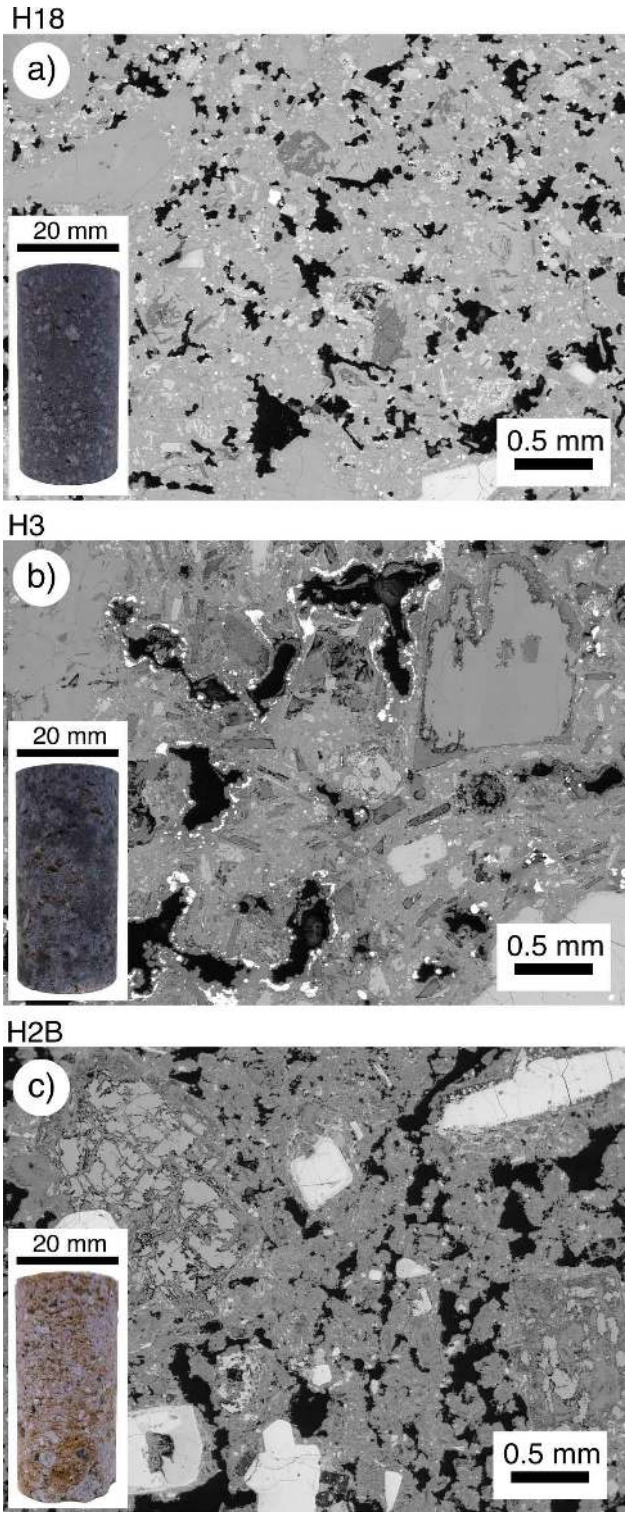

293

294 **Figure 2.** Backscattered scanning electron microscope images of three andesites from La

295 Soufrière de Guadeloupe (Eastern Caribbean, France) selected to represent the range of

296 observed alteration: (a) relatively unaltered – H18, (b) moderately altered – H3, and (c) highly

297 altered – H2B. Black – porosity; grayscale – rock groundmass. Insets show photographs of
298 the 20 mm-diameter cylindrical samples.
299

Mineral	H2A	H2B	H3	H4A	H5A	H6	H14	H15	H18	H19	H20	H21	H22	H25	H29	WP1285	WP1317
Plagioclase	56.7	12.3	46.6	23.3	41.3	30.0	60.7	22.5	61.2	22.0	28.7	24.2	59.5	38.7	62.4	64.7	61.6
Clinopyroxene	8.7	3.4	5.6	4.9	5.2	6.4	6.3	7.3	8.4	5.0	8.9	12.4	8.9	5.3	7.8	5.2	5.9
Orthopyroxene	10.8	9.5	11.8	11.8	11.1	10.8	8.6	9.2	12.2	10.2	15.0	19.3	13.6	10.2	11.2	13.2	15.6
(Ti-) Magnetite	0.7	-	0.8	-	-	-	0.8	-	2.9	-	2.4	3.1	0.8	-	2.7	3.5	0.7
Quartz*	1.0	0.5	0.6	0.6	0.5	0.5	1.7	0.7	0.7	1.7	0.3	0.2	0.6	0.3	0.4	0.2	0.7
Cristobalite*	11.3	12.8	10.6	11.8	13.0	11.1	13.5	10.2	11.7	9.5	11.4	11.7	10.6	9.8	12.4	-	-
Tridymite*	-	-	-	-	-	-	-	0.7	-	-	-	-	-	-	-	13.2	13.2
Hematite*	-	-	-	-	-	-	3.4	-	2.8	2.4	-	-	-	-	3.1	-	-
Pyrite*	3.5	-	3.8	2.3	-	-	-	-	-	-	-	0.4	3.1	0.6	-	-	-
Alunite*	-	-	-	-	-	-	-	-	-	-	-	-	-	-	-	-	2.4
Na-Alunite*	1.4	1.6	2.8	1.3	5.4	5.1	5.1	15.0	-	14.2	0.5	0.5	-	9.8	-	-	-
Gypsum*	-	-	-	0.7	-	-	-	-	-	-	0.8	1.2	-	-	-	-	-
Kaolinite*	6	59.7	17.4	43.3	23.5	36.0	< 1	34.3	-	2.0	2.0	2.0	< 1	25.3	-	-	-
Talc*	-	-	-	-	-	-	-	-	-	-	-	-	2.9	-	-	-	-
Opal-A*	-	-	-	-	-	-	-	-	-	33.0	30.0	25.0	-	-	10.0	-	-

300

301 **Table 1.** Mineral contents, measured by X-ray powder diffraction and refined using Raman
302 spectroscopy and optical microscopy, of the 17 blocks collected for this study (sampling
303 locations shown in Figure 1b). Values in wt.%. Asterisk denotes a secondary/alteration
304 mineral.
305

306 4.2 Mechanical data

307 Representative uniaxial stress-strain curves for selected samples are shown in Figure
308 3a. Stress is first a non-linearly increasing function of strain, often attributed to the closure of
309 pre-existing microcracks. This stage is followed by a quasi-linear elastic stage. In the next stage,
310 stress is a non-linearly decreasing function of strain, a result of the initiation, propagation, and
311 coalescence of microcracks. Finally, a stress drop signals the formation of a macroscopic shear
312 fracture. Uniaxial compressive strength and Young's modulus are plotted as a function of
313 connected porosity in Figures 3b and 3c, respectively (data available in Table 2). We first note

that the connected porosity of our samples varies from 0.12 to 0.43. The uniaxial compressive strength and Young's modulus of our sample suite varies from ~3.5 to ~150 MPa and from ~1 to ~43 GPa, respectively (Figure 3). Our data show that uniaxial compressive strength and Young's modulus both decrease as a function of increasing porosity (Figure 3).

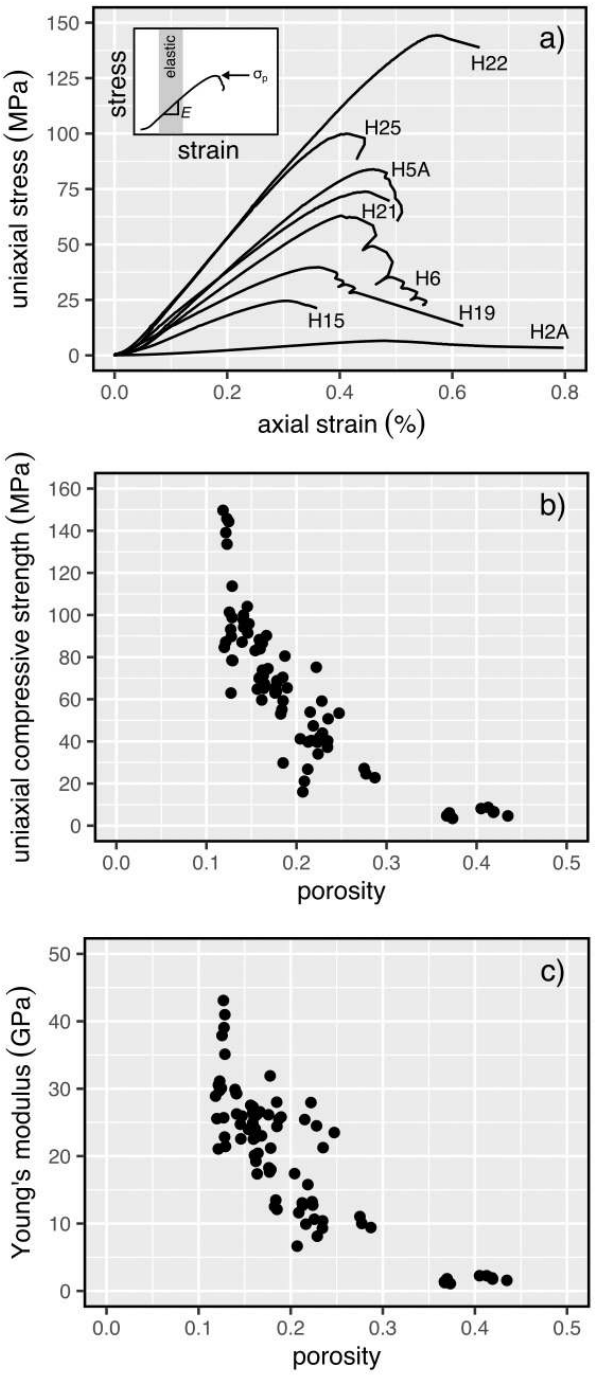

320 **Figure 3.** (a) Representative stress-strain curves for selected andesite samples from La
321 Soufrière de Guadeloupe (Eastern Caribbean, France). Inset shows an isolated curve
322 indicating from where the Young's modulus (the slope of the stress-strain curve), E, was
323 determined (the quasi-linear elastic stage is indicated by the gray zone). Also labeled is the
324 uniaxial compressive strength, σ_p, which is the maximum axial stress the sample attained
325 prior to macroscopic failure (signaled by the stress drop). Uniaxial compressive strength (b)
326 and Young's modulus (c) as a function of connected porosity (data available in Table 2).
327

Sample	Connected porosity	Uniaxial compressive strength (MPa)	Young's modulus (GPa)	Percentage of secondary minerals
H2A_2	0.18	63.7	31.9	23.2
H2A_5	0.19	80.5	25.5	23.2
H2A_6	0.19	65.4	25.8	23.2
H2A_11	0.19	59.3	24.4	23.2
H2A_12	0.18	70.4	28.0	23.2
H2B_3	0.42	6.6	1.8	74.6
H2B_10	0.42	6.4	1.9	74.6
H2B_11	0.41	8.7	2.3	74.6
H2B_12	0.41	8.1	2.3	74.6
H2B_15	0.43	4.6	1.6	74.6
H3_3	0.16	70.3	27.3	35.2
H3_7	0.16	69.9	24.9	35.2
H3_8	0.16	64.8	27.5	35.2
H3_11	0.16	59.7	24.0	35.2
H3_13	0.16	71.2	26.2	35.2
H4A_2	0.23	40.3	10.4	60.0
H4A_4	0.23	42.0	10.6	60.0
H4A_6	0.23	43.9	8.1	60.0
H4A_8	0.23	37.2	9.3	60.0
H4A_9	0.22	40.4	9.9	60.0
H5A_2	0.16	88.3	26.4	42.4
H5A_3	0.16	86.6	22.8	42.4
H5A_5	0.16	83.9	22.5	42.4
H5A_8	0.18	68.8	21.2	42.4
H5A_10	0.17	74.5	23.0	42.4
H6_6	0.18	55.1	13.5	52.7
H6_9	0.18	68.0	18.0	52.7
H6_9	0.18	53.0	12.5	52.7
H6_12	0.18	64.2	17.6	52.7
H6_13	0.18	63.0	18.3	52.7
H14_2	0.18	65.4	26.1	23.7

H14_3	0.21	21.1	11.6	23.7
H14_5	0.21	26.8	13.1	23.7
H14_6	0.19	29.8	12.1	23.7
H14_10	0.21	16.1	6.6	23.7
H15_3	0.28	24.6	10.0	60.9
H15_4	0.28	27.1	11.0	60.9
H15_5	0.29	22.8	9.4	60.9
H18_3	0.13	101.3	37.9	15.2
H18_4	0.13	89.8	39.1	15.2
H18_5	0.13	98.8	41.0	15.2
H18_6	0.13	93.2	43.1	15.2
H18_7	0.13	113.7	35.1	15.2
H19_3	0.21	39.7	12.7	62.8
H19_8	0.22	47.4	15.8	62.8
H19_9	0.22	34.1	12.7	62.8
H19_12	0.20	41.2	17.4	62.8
H19_15	0.22	39.6	13.2	62.8
H20_2	0.37	4.8	1.2	45.0
H20_3	0.37	4.4	1.3	45.0
H20_7	0.37	4.6	1.4	45.0
H20_8	0.37	6.1	1.8	45.0
H20_10	0.37	3.4	1.1	45.0
H21_3	0.17	90.2	26.6	41.0
H21_8	0.16	65.2	17.4	41.0
H21_11	0.16	86.9	25.8	41.0
H21_12	0.16	73.8	19.2	41.0
H21_13	0.16	87.2	20.1	41.0
H22_2	0.12	145.7	29.7	17.2
H22_3	0.12	144.3	30.1	17.2
H22_4	0.12	139.1	30.5	17.2
H22_5	0.12	149.7	28.9	17.2
H22_6	0.12	133.6	31.1	17.2
H25_2	0.14	99.9	29.3	45.8
H25_4	0.14	97.7	29.3	45.8
H25_5	0.14	94.2	26.2	45.8
H25_9	0.14	87.1	29.9	45.8
H25_12	0.15	83.1	24.0	45.8
H29_2	0.22	53.9	25.4	25.9
H29_8	0.23	59.1	24.5	25.9
H29_9	0.22	75.2	27.9	25.9
H29_12	0.25	53.4	23.5	25.9
H29_16	0.24	50.7	21.3	25.9
WP1285_2	0.13	78.5	22.8	13.4
WP1285_8	0.13	63.0	25.7	13.4
WP1285_10	0.13	78.3	21.4	13.4
WP1285_11	0.12	87.2	21.1	13.4
WP1285_15	0.12	84.6	25.6	13.4
WP1317_2	0.16	67.3	20.4	16.3
WP1317_6	0.16	84.5	24.7	16.3
WP1317_7	0.15	91.5	22.6	16.3

WP1317_8	0.15	95.8	25.9	16.3
WP1317_12	0.15	104.0	24.7	16.3

328

329 **Table 2.** Connected porosity, uniaxial compressive strength, Young's modulus, and the
330 percentage of secondary minerals (i.e. alteration) for the samples prepared for this study.
331 Sample locations are provided in Figure 1b (site descriptions and GPS coordinates are
332 available in the Supplementary Information).

333

334 Samples from three blocks were selected for triaxial compression experiments: a
335 relatively unaltered block (H18), a moderately altered block (H3), and a very altered block
336 (H2B). The microstructure of these samples is provided in Figure 2 and their mineral
337 componentry in Table 1. The percentages of secondary minerals (determined using the XRPD
338 data; Table 1) for these rocks are 15.2, 35.2, and 74.6%, respectively. Triaxial experiments were
339 performed on H18 samples at effective pressures of 0, 2.5, 5, 10, and 15 MPa (Figure 4a), on
340 H3 samples at effective pressures of 0, 2.5, 5, and 7.5 MPa (Figure 4b), and on H2B samples at
341 effective pressures of 0, 0.5, 1, and 2 MPa (Figure 4c) (data available in Table 3). Different
342 effective pressures were chosen for the different samples in an attempt to ensure the brittle
343 behavior required to calculate the cohesion and angle of internal friction. Blocks H18 (Figure
344 4a) and H3 (Figure 4b) were brittle over the chosen range of effective pressures. The
345 compressive strength of blocks H18 and H3 increased as a function of increasing effective
346 pressure: H18 increased from 65.4 to 143.8 MPa and H3 increased from 31.5 to 54.8 MPa as
347 effective pressure was increased from 0 to 15 and 7.5 MPa, respectively (Figure 4). The stress-
348 strain curves for block H2B are very different to those for blocks H18 and H3 (Figure 4). Subtle
349 strain softening associated with brittle behavior was observed for the experiments performed at
350 effective pressures of 0 and 0.5 MPa, but no strain softening was seen at 1 and 2 MPa,
351 suggestive of ductile behavior (Figure 4c).

352 The cohesion and angle of internal friction calculated using these triaxial data
353 (excluding the two ductile H2B experiments), necessary for the large-scale numerical modeling,
354 were 14.8 MPa and 46.7° for H18, 7.1 MPa and 37.7° for H3, and 0.4 MPa and 42.5° for H2B,
355 respectively (Figure 4). The method for determining these values is explained in the
356 Supplementary Information.
357

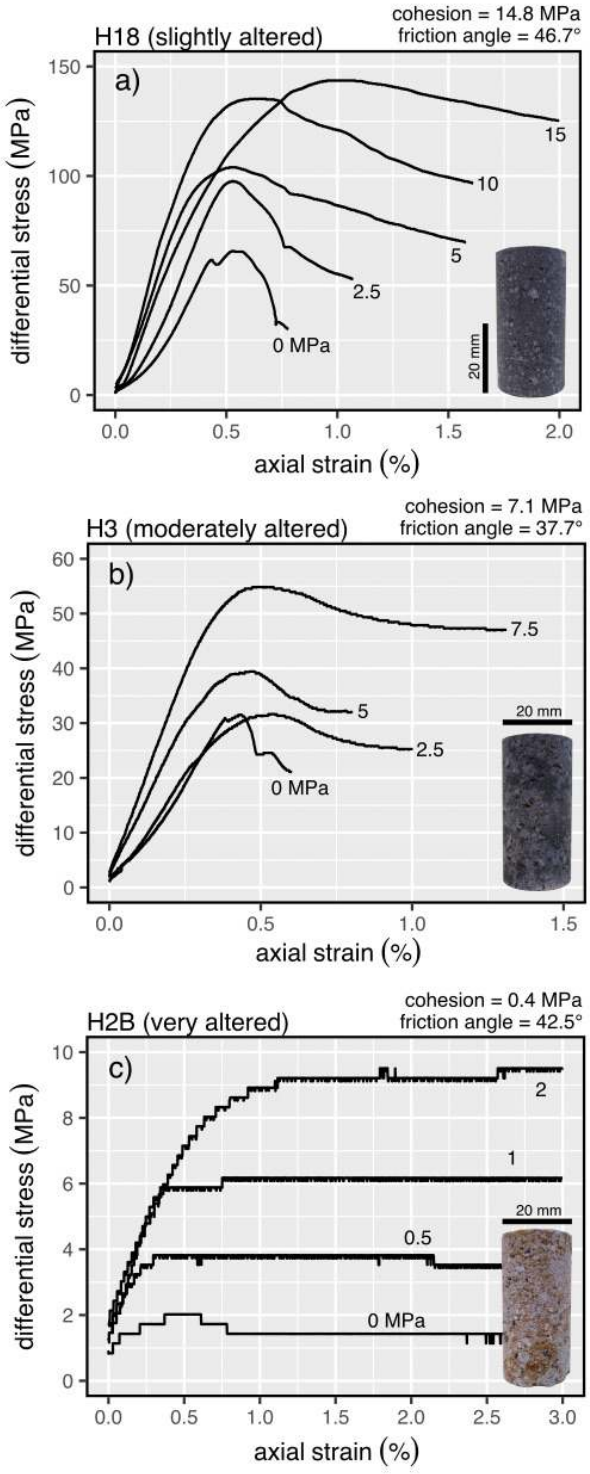

Figure 4. Stress-strain curves for andesites from La Soufrière de Guadeloupe (Eastern Caribbean, France) deformed under different effective pressures (given by the number adjacent to each curve). (a) Relatively unaltered sample H18. (b) Moderately altered sample H3. (c) Very altered sample H2B. Differential stress is the axial stress minus the confining

pressure. Insets show photographs of the 20 mm-diameter cylindrical samples. The values of cohesion and internal friction angle, calculated using these data, are also provided for each of the three rocks.

Sample	Connected porosity	Percentage of secondary minerals	Pore fluid pressure (MPa)	Confining pressure (MPa)	Effective pressure (MPa)	Peak differential stress (MPa)
H18_11	0.13	15.2	0 (wet)	0	0	65.7
H18_10	0.14	15.2	10	12.5	2.5	97.7
H18_2	0.12	15.2	10	15	5	104.0
H18_8	0.12	15.2	10	20	10	135.2
H3_14	0.16	35.2	0 (wet)	0	0	31.5
H3_12	0.15	35.2	10	12.5	2.5	31.7
H3_4	0.15	35.2	10	15	5	39.4
H3_5	0.16	35.2	10	17.5	7.5	54.9
H2B_7	0.44	74.6	0 (wet)	0	0	2.0
H2B_8	0.44	74.6	10	10.5	0.5	3.8
H2B_6	0.39	74.6	10	11	1	-
H2B_5	0.38	74.6	10	12	2	-

Table 3. Experimental summary for the triaxial deformation experiments (and wet uniaxial experiments) performed on relatively unaltered (H18), moderately altered (H3), and very altered (H2B) andesites from La Soufrière de Guadeloupe (Eastern Caribbean, France). Sample locations are provided in Figure 1b (site descriptions and GPS coordinates are available in the Supplementary Information) and microstructural images are provided in Figure 2.

5 Discussion

5.1 Hydrothermal alteration and mineral precipitation

Volcanic andesitic systems discharging acid-chloride-sulfate hydrothermal fluids (Browne, 1978; Ellis and Mahon, 1977; Taran and Kalacheva, 2020) are typically characterized by either propylitic alteration, resulting from the rapid ascension of acidic fluids and the lack

of time available for neutralization (Taran and Kalacheva, 2020), or intermediate to advanced argillic alteration in zones where fluids can circulate. The samples measured for this study were sourced from (1) zones proximal to summit fumarolic vents that tap the central zone characterized by the rapid ascent of steam separated from a boiling hydrothermal aquifer (Brombach et al., 2000; Moretti et al., 2020) (e.g., H18–22; Table 1) and (2) from zones far from currently active fumarolic zones, where the shallow groundwaters are heated via conduction and mixed with Na-Cl liquids from the hydrothermal aquifer (Brombach et al., 2000; Villemant et al., 2014) (e.g., those sampled from the collapse scar of the 2009 landslide: H2A, H2B, H3, H4A, H5A, H6, H25, and H29; Table 1) (Figure 1b).

The secondary mineral assemblage in our samples (Table 1) is essentially the same as that found in the debris avalanche deposits to the southwest of La Soufrière (Salaün et al., 2011). However, the debris-avalanche deposits investigated by Salaün et al. (2011) contain abundant smectite, whereas the samples collected for this study contain kaolinite and no smectite (Table 1). The presence of kaolinite, a key mineral in the argillic alteration facies, typically indicates fluid-rock interaction at relatively low fluid temperatures (< 150–200 °C) and a pH of ~4.5–6 (Fulignati, 2020; Inoue, 1995), but can also occur in the advanced argillic alteration facies (pH < 3; temperatures up to about 300 °C). The altered samples analyzed in this study therefore represent a more advanced stage of hydrolysis reactions than the smectite-bearing products from the Holocene debris-avalanche deposits described in Salaün et al. (2011), indicating that the rocks analyzed here were altered by hydrothermal fluids with a higher H^+ activity that led to complete alkali leaching.

The most abundant secondary minerals are cristobalite, amorphous silica, natroalunite, and kaolinite (Table 1). Cristobalite is a silica polymorph stable at low-pressure and high-temperature in its cubic β-form (Schipper et al., 2020). Because it is kinetically favored, metastable cristobalite is commonly found in preference to quartz in lava domes, where it

405 precipitates from a vapor-phase enriched in magmatic components or results from groundmass
406 devitrification (Horwell et al., 2013; Martel et al., 2021; Schipper et al., 2020). Our samples
407 contain tetragonal α-cristobalite, suggesting a final temperature lower than 240 °C, the nominal
408 temperature for the transition from β- to α-cristobalite (Damby et al., 2014). Schipper et al.
409 (2020) identified a lower and broader range for the β-α transition in volcanic cristobalites
410 (~150–200 °C), which overlaps with the temperature interval inferred by the presence of
411 kaolinite. The cristobalite in the studied samples precipitated onto pore walls (see Figure 2 and
412 the Supplementary Information) and so we consider that it predominately formed by vapor
413 deposition. Amorphous silica (opal-A) partially to completely replaced the plagioclase
414 phenocrysts (see Figure 2 and the Supplementary Information), as often observed in acid-sulfate
415 alteration zones (McCollom et al., 2013).

416 Alunite is a characteristic family of sulfate minerals produced by hypogene magmatic-
417 hydrothermal and steam-heated alteration or supergene processes (Rye et al., 1992). As such it
418 is commonly found in the alteration products of rhyolitic to andesitic rock compositions,
419 including surficial solfataric or acid hot spring environments. Alunite and natroalunite are the
420 two most common minerals of the alunite group (Stoffregen et al., 2000). Only the volcanic
421 bomb from the 1976–1977 eruption (sample WP1317) contains alunite, whereas natroalunite is
422 commonly observed (Table 1). Natroalunite is the high temperature end-member of the alunite
423 group and typically forms at 200–350 °C, but is also stable at 380–450 °C (Henley and Berger,
424 2011; Meyer and Hemley 1967). Natroalunite precipitates from an acidic (pH < 4) fluid with a
425 high sulfate content and high [Na]/[K] ratio (Hemley et al., 1969; Stoffregen and Cygan, 1990).
426 Natroalunite precipitation requires fluids with [Na]/[K] about 100 (at pH = 3; Deyell and
427 Dipple, 2005), much higher than measured in circulating fluids and in whole rock and
428 groundmass compositions at La Soufrière (Boudon et al., 2008; Metcalfe et al., 2021; Villemant
429 et al., 2005), suggesting that equilibrium was not obtained or that the fluids responsible are

different from those discharged at the surface (Deyell and Dipple, 2005). If the fluids are different, acidic Na-Cl-SO_4 fluids would be required, which form H_2S and H_2SO_4 following the interaction between Na-Cl waters and elemental sulfur at depth (Taran and Kalacheva, 2020). This hypothesis is compatible with the observation that highly acidic chlorine-sulfate rich fluids (pH < 1) have been rising and circulating within the dome as of early 1998, forming acid ponds within summit craters (Komorowski et al., 2005, Rosas-Carbajal et al., 2016; Villemant et al., 2014). Alternative hypotheses include the interaction of Na-Cl neutral water (water/rock volume ratio >> 1) with rocks already showing advanced argillic alteration, and that the rocks collected represent old and buried solfataric fields (Marini et al., 2003) resulting from previous volcanic cycles.

We conclude that the observed secondary mineral assemblages (Table 1) are the result of intense fluid-rock interactions. Advanced argillic alteration of the shallow portion of the edifice was promoted by the efficient circulation of cooled (below 350 °C, and down to 150°C–200 °C), acidic (pH < 4) hydrothermal fluids, possibly mixed with meteoric waters. The alteration assemblages observed at La Soufrière are similar to those commonly identified at domes and craters of active volcanoes worldwide (Heap et al., 2019; Zimbelman et al., 2005; Yilmaz et al., 2021), although the rocks from Mt Unzen volcano (Japan) were overprinted by propylitic alteration (Yilmaz et al., 2021), not observed here. Multiple reaction paths and variable alteration intensity reflect a variable degree of reaction progress. For a given alteration rate, reaction progress will increase as exposure to altering fluids and pathway length increase, or as water flow and water/rock volume ratio decrease. Variations in these environmental parameters simply reflect the heterogeneity and structural complexity of the dome and thus the complex architecture of the hydrothermal system, as revealed by geological and geophysical data (Brothelande et al., 2014; Jessop et al., 2021; Moretti et al., 2020; Nicollin et al., 2006; Rosas-Carbajal et al., 2016; Tamburello et al., 2019). In particular, the complex 3D geometry

of large faults and fractures in the dome allow for the efficient drainage of fluids and the compartmentalization of supergene and hypogene alteration. In such an environment: (1) intermediate to advanced argillic alteration will develop preferentially along discontinuities favoring fluid circulation, leading to the formation of low-strength layers dominated by clay and sulfate minerals; (2) partial edifice collapse or erosion favored in these weakened zones will expose pyrite-rich zones of the hydrothermal system below the water table and promote the deepening of supergene oxidation and the alteration aureole (as seen in the rain-triggered landslide in 2009; Rosas-Carbajal et al., 2016); and (3) H_2S will be easily released by deeper, boiling fluids or by the disproportionation of magmatic SO_2 to H_2S and aqueous sulfate during the condensation of magmatic vapor plume at intermediate depths.

5.2 The influence of porosity and alteration on uniaxial compressive strength

New mechanical data show that the uniaxial compressive strength and Young's modulus of variably-altered andesites from La Soufrière both decrease as a function of increasing porosity (Figure 3), in accordance with previous studies on volcanic rocks (Heap et al., 2014a, 2020a; Heap and Violay, 2021; Mordensky et al., 2018; Schaefer et al., 2015; Zhu et al., 2016). We compare our new data with those previously published for andesites in Figure 5a and 5b, which show that the data for the rocks from La Soufrière are in broad agreement with those previously published. This comparison shows that the andesites forming La Soufrière are generally more porous, and therefore weaker (Figure 5a) and softer (Figure 5b), than andesites from other stratovolcanoes (the block with the lowest porosity, H22, has a porosity of 0.12). Indeed, muon tomography data have shown that the material forming the dome at La Soufrière is typically low-density (typically $\leq$ 1500 $kg.m^{-3}$; Lesparre et al., 2012; Rosas-Carbajal et al., 2017) and, therefore, likely comprises high-porosity rocks. However, we note that the relative abundance of high-porosity rocks with a low strength and a low Young's

480 modulus from La Soufrière may be a consequence of sampling only 17 blocks. In other words,
481 low-porosity rocks may exist at La Soufrière and, if many more blocks were sampled, maybe
482 the data would encompass a similar range to the compiled dataset for other volcanoes.
483

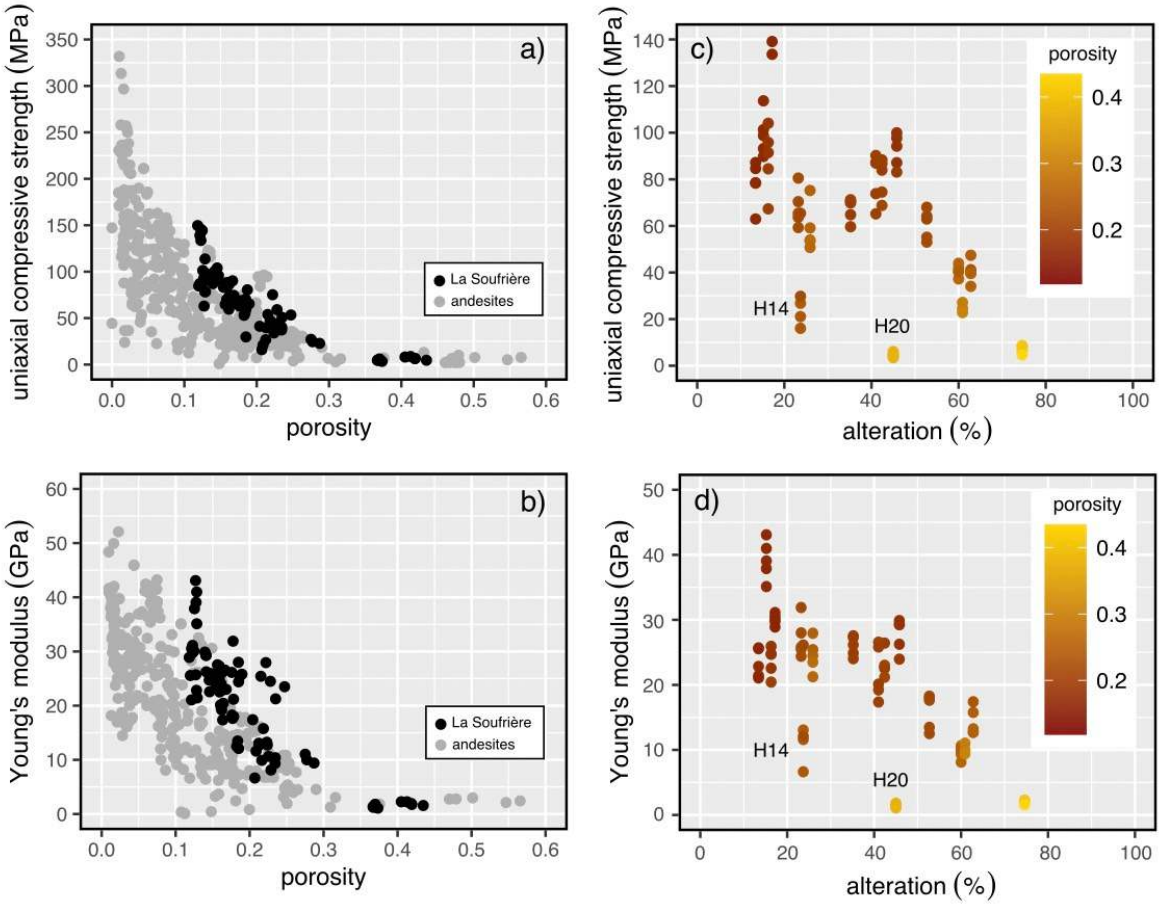

484

485 **Figure 5.** (a) Uniaxial compressive strength and (b) Young's modulus as a function of
486 porosity for andesites from La Soufrière de Guadeloupe (Eastern Caribbean, France) and from
487 volcanoes worldwide (data from: Karaman and Kesimal, 2015; Heap et al., 2014b; Siratovich
488 et al., 2014; Wyering et al., 2014; Heap et al., 2015a; Mordensky et al., 2018; Harnett et al.,
489 2019; Kennedy et al., 2020; Heap and Violay, 2021). Uniaxial compressive strength (c) and
490 Young's modulus (d) as a function of alteration (the percentage of secondary minerals).
491 Symbol color indicates the connected porosity (red colors indicate low porosity and yellow

colors indicate high porosity). Outliers—blocks H14 and H20—are labelled on panels (c) and (d).

Of interest to the goal of this study is whether hydrothermal alteration has influenced the compressive strength and Young's modulus of the materials collected. Our triaxial data highlight that alteration (percent of secondary minerals) reduces rock cohesion, but does not systematically influence the angle of internal friction (Figure 4). Experimental studies have shown that alteration can influence the strength of volcanic rock (del Potro and Hürlimann, 2009; Farquharson et al., 2019; Frolova et al., 2014; Heap et al., 2020b, 2021b, Mordensky et al., 2018, 2019; Wyering et al., 2014). The type of alteration, porosity increasing dissolution and alteration to clay (del Potro and Hürlimann, 2009; Farquharson et al., 2019; Opfergelt et al., 2006; Watters and Delahaut, 1995) or porosity decreasing mineral precipitation (Heap et al., 2020b, 2021), dictates whether the alteration decreases or increases the strength and Young's modulus of the rock. Figure 5c and 5d show plots of uniaxial compressive strength and Young's modulus, respectively, as a function of the percentage of secondary minerals for the rocks from La Soufrière. The symbols in Figure 5c and 5d are color-coded to show their porosity: red colors indicate low porosity and yellow colors indicate high porosity. Although there are two notable outliers, Figure 5c and 5d, respectively, show that uniaxial compressive strength and Young's modulus decrease as a function of increasing hydrothermal alteration. Uniaxial compressive strength and Young's modulus are reduced from ~60–140 to < 10 MPa and from 20–45 to < 5 GPa as alteration increases from ~16–18 to ~75% (Figure 5c and 5d). The low uniaxial compressive strengths and Young's moduli of the two relatively unaltered blocks that form the most obvious outliers (H14 and H20) can be explained by meso-scale fractures found within sample H14 (sample photographs are provided in the Supplementary Information) and the high porosity of sample H20, respectively. Although the data in Figure 5c

and 5d suggest that an increase in alteration results in a decrease in strength and Young's modulus, it is difficult to untangle the influence of porosity. In other words, are the weak samples weak because of alteration or are the more porous samples simply more altered because of their higher surface area available for rock-fluid interactions? Indeed, our data do show that, in general, alteration increases as a function of increasing porosity. Although laboratory-controlled hydrothermal alteration experiments (Farquharson et al., 2019) are required to definitively answer this question, we contend here that the observed alteration served to reduce the strength and Young's modulus of these andesites from La Soufrière, regardless of their porosity, due to the presence of abundant clay minerals, phases considered to reduce the strength of volcanic rocks (del Potro and Hürlimann, 2009; Nicolas et al., 2020; Opfergelt et al., 2006; Watters and Delahaut, 1995).

5.3 Influence of alteration on the stability of La Soufrière de Guadeloupe: large-scale numerical modeling

We used the open-source hydro-thermo-mechanical modeling code LaMEM (Lithosphere and Mantle Evolution Model; https://bitbucket.org/bkaus/lamem/src/master/; Kaus et al., 2016), which models the non-linear, visco-elastoplastic deformation of rocks, to investigate the influence of upscaling and alteration on the stability of La Soufrière. This model has recently been used to model large-scale volcano deformation (Heap et al., 2021a). Mathematically, the model solves a coupled system of conservation equations, the conservation equations of momentum and mass. The various deformation mechanisms are connected in an additive constitutive relationship, where the total strain rate is the sum of the individual strain rates of elastic, viscous, and plastic deformation. LaMEM uses the Drucker-Prager failure criterion to determine the magnitude of the plastic strain rate. Numerically, LaMEM uses a staggered-grid finite difference method for discretization and a marker-and-cell method to

assign and track rock properties within a Eulerian advection framework (Harlow and Welch, 1965). This approach enables the model to attain the large deformations required in, for example, salt tectonics, continental collision, and magmatic systems (Baumann et al., 2014; Pusok and Kaus, 2015; Reuber et al., 2018). The ability to model large deformations is seen here as an advantage of LaMEM over commonly-used commercial packages such as FLAC (by Itasca Consulting Group), RS2 (by Rocscience), and PLAXIS 2D (by Virtuosity). We refer the reader to Kaus et al. (2016) and the Supplementary Information for a more detailed description of LaMEM.

Models were run on simplified 2D North-South cross-sections of the volcano (643 km Easting), built using the geomIO tool (Bauville and Baumann, 2019). The model domain was first separated into deformable and non-deformable domains, guided by geological observations and the recent electrical survey of Rosas-Carbajal et al. (2016). The models have a dimension of 2000 × 800 m, a model resolution of 4 × 3 m, free-slip boundary conditions at the sides, and a free surface at the top. All our models assumed an entirely liquid saturated volcano. The average topographic height was used as the reference surface for determining the hydrostatic pressure, p_h, using $p_f = p_h + \lambda_i (p_{lith} - p_h)$, where p_f and p_{lith} are the pore fluid and lithostatic pressure, respectively, and λ_i is the pore fluid pressure ratio. Following Heap et al. (2021a), we assumed a value of 0.2 for λ_i (Table 4). To account for the uncertainty in λ_i, additional models using λ_i = 0.4 are provided in the Supplementary Information. We highlight that, although the assumption of complete volcano saturation is an oversimplification (Ball et al., 2015, 2018; Hurwitz et al., 2003), the main goal of our modeling was to understand, all else being equal, whether hydrothermal alteration is a contributing factor to the deformation observed at La Soufrière. Further, the distribution of liquid-saturated and dry zones within the volcano is currently poorly constrained. However, using the average topographic height as the

reference surface resulted in a "dry" volcano summit with a pore fluid pressure of zero (see Supplementary Information for further details).

By modifying the segmentation of the deformable domain, we prepared three cross-sections: (1) a homogeneous volcano, (2) a volcano containing alteration zones identified by the electrical conductivity data of Rosas-Carbajal et al. (2016), and (3) a volcano in which we artificially enlarged the highly altered zone identified by Rosas-Carbajal et al. (2016). Zones within the volcano cross-sections were designated as either slightly altered (V3), moderately altered (V2), or highly altered (V1) (Figures 6a-d). Zones V3, V2, and V1 were assigned the mechanical properties of samples H18, H6, and H2B, respectively, the three blocks chosen to represent relatively unaltered, moderately altered, and highly altered rock (Figure 2; Table 1). The laboratory data used in the modeling were: water-saturated bulk density, Young' modulus, cohesion, and the angle of internal friction. Poisson's ratio, not measured here, was assumed to be 0.2 (as recommended by Heap et al., 2020a). The model parameters for V3, V2, and V1 are provided in Table 4. As the models are dynamic, we must decide when the models reach a quasi-steady state and can be compared (see Baumann and Kaus, 2015). Here, we stop the models after an initial deformation phase that is dominated by an elastic response. For each of the three modeled scenarios, we ran one model in which we used the laboratory data and one model in which we used upscaled values of the laboratory data (Table 4).

	V1 (highly altered)	**V2 (moderately altered)**	**V3 (relatively unaltered)**
Laboratory-scale input parameters			
Bulk density(kg/m³)	1900	2400	2500
Young's modulus (GPa)	0.4	9.6	20.3
Poisson's ratio	0.2	0.2	0.2
Cohesion (MPa)	0.4	7.1	14.8
Internal friction angle (°)	42.5	37.7	46.7
Pore fluid pressure ratio	0.2	0.2	0.2
Upscaled input parameters			
Bulk density(kg/m³)	1900	2400	2500
Young's modulus (GPa)	0.2	3.9	8.3
Poisson's ratio	0.3	0.3	0.3

Cohesion (MPa)	0.67	1.09	2.02
Internal friction angle (°)	30.1	33.5	46.4
Pore fluid pressure ratio	0.2	0.2	0.2

585

586 **Table 4.** Laboratory-scale and upscaled input parameters for the numerical modeling
587 performed using hydro-thermo-mechanical modeling code LaMEM (Lithosphere and Mantle
588 Evolution Model).

589

590 The laboratory-scale Young's modulus and Poisson's ratio were upscaled using
591 empirical relationships for Young's modulus (Hoek and Diederichs, 2006) and Poisson's ratio
592 (Vásárhelyi, 2009) that account for rock-mass structure using the Geological Strength Index
593 (GSI), as described in Heap et al. (2020a). Following Heap et al. (2020a), GSI was assumed to
594 be 55 and the damage parameter in the Hoek-Diederichs equation was considered zero. The
595 cohesion and angle of internal friction were upscaled by transforming the generalized form of
596 the Hoek-Brown failure criterion to the Mohr-Coulomb failure criterion (as in Hoek et al.,
597 2002). We used the mean uniaxial compressive strength of samples H18, H6, and H2B for
598 layers V3, V2, and V1, respectively. The empirical fitting parameter m_i required for the
599 generalized Hoek-Brown failure criterion was determined from the triaxial data (Figure 4) using
600 RocData (Rocscience; https://www.rocscience.com). To do so, we again assumed a GSI of 55
601 and a damage parameter of zero. Since a depth is required to upscale the cohesion and angle of
602 internal friction, we selected a depth half of that between the summit of the volcano and the top
603 of the undeformable zone in the model (275 m). The upscaled model parameters for V3, V2,
604 and V1 are provided in Table 4. A more detailed description of the upscaling methods can be
605 found in the Supplementary Information.

606

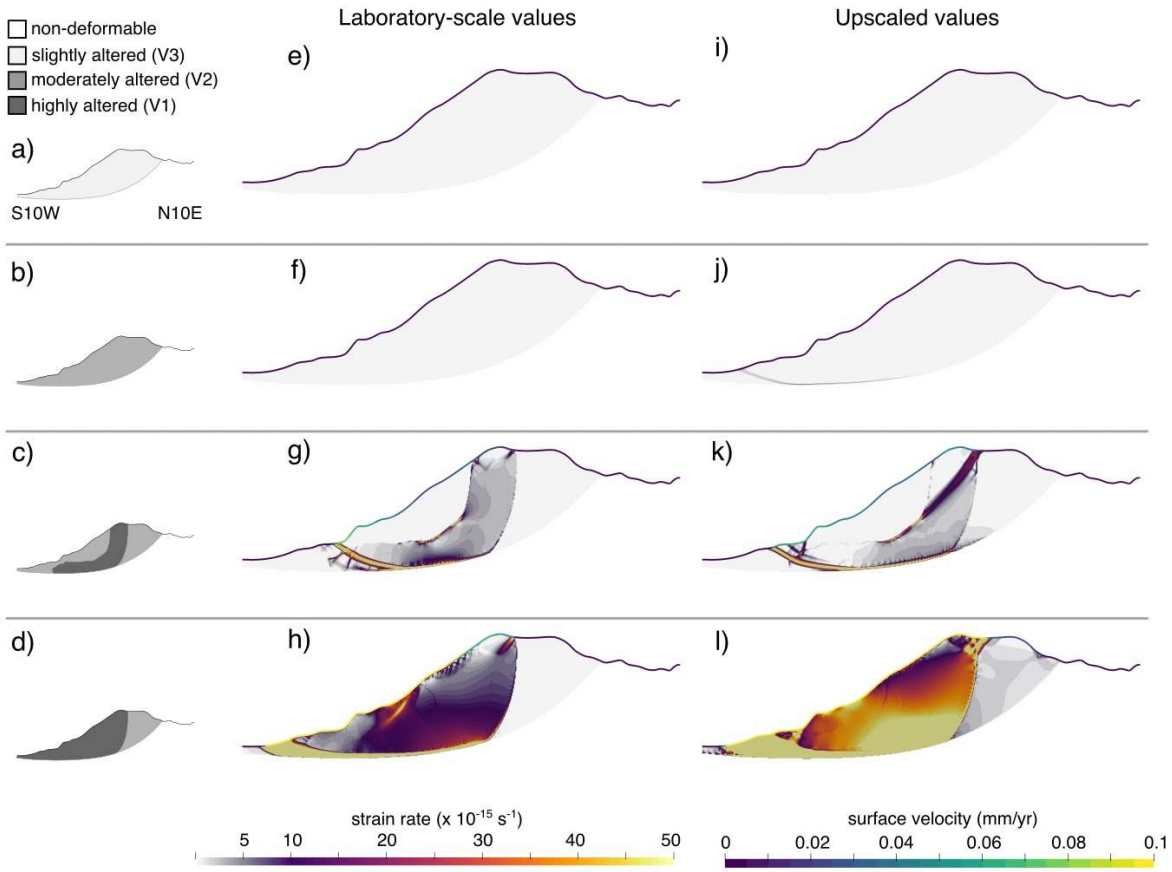

607

608 **Figure 6.** Results of the large-scale 2D numerical modeling designed to better understand the
609 influence of alteration on the stability of La Soufrière de Guadeloupe Eastern (Caribbean,
610 France). Panels (a-d) show the model setup, in which white, light grey, grey, and dark grey
611 indicate non-deformable, slightly altered (V3), moderately altered (V2), and highly altered
612 (V1) zones. Panels (e-h) and (i-l) show the model results for the models run using laboratory-
613 scale and upscaled mechanical properties, respectively. The color of the line representing the
614 surface of the volcano indicates the surface velocity (mm/yr) and the color inside the volcano
615 indicates the strain rate (s^{-1}).

616

617 The model results, the velocity magnitude at the surface and the 2nd invariant of the
618 deviatoric strain rate tensor, which we refer to as the strain rate, within the deformable domain,
619 are presented in Figure 6. The strain rate allows us to understand whether the deformation is

widespread or localized, and the velocity at the surface can be compared to geophysical data. Figures 6e-h and 6i-l show model runs using the laboratory-scale and upscaled values, respectively. We first highlight that our results emphasize the importance of using upscaled values for large-scale modeling. Not only are the strain rates and velocities much lower when using the laboratory-scale values, but the deformation also manifests slightly differently (Figure 6).

To discuss the influence of alteration, we will restrict our discussion to the upscaled models (Figures 6i-l). We first note that strain rates and velocities are low in the homogenously altered volcanoes, that deformation is largely restricted to the surface and the base of southern slope, and that there is little difference in strain rates and velocities when the alteration is increased from slightly to moderately altered (Figures 6i and 6j). When the highly-altered zone guided by the recent electrical survey of Rosas-Carbajal et al. (2016) is included, the strain rates and velocities increase significantly (Figure 6k). Surface velocities increase from < 0.01 to ~0.05 mm/yr and a large listric, concave-upward sliding surface emerges, which stretches from the top of the dome to near the base of the southern flank (Figure 6k). A localized slip surface at the base of the deformable domain and two smaller slip surfaces also emerge near the base of the southern flank (Figure 6k). Therefore, the inclusion of the highly altered zone, the consequence of pervasive alteration resulting from the circulation of acid hydrothermal fluids (Rosas-Carbajal et al., 2016), has significantly increased volcano deformation rates and therefore decreased the stability of the volcano. As outlined above, recent manifestations of increased hydrothermal activity, such as fumaroles and hot springs (Moretti et al., 2020; Jessop et al., 2021), also provide evidence that the measured ground deformation is, in part, due to the alteration of the rock forming the dome. Continuous and campaign Global Navigation Satellite System (GNSS) measurements over ~20 years show that the dome is sliding at a rate of 0.3–0.7 cm/yr (Moretti et al., 2020). Therefore, although our modeling captures the dynamics of the

deformation of the southern flank, our simplified 2D model setup (Figure 6) underestimates the deformation measured at the volcano. This underestimation is likely the result of the presence of large-scale faults, discontinuities, extremely weak clay-rich layers, and zones of high pore pressure, not included in our modeling. Indeed, the strain rate in the southern flank increases when we increase the pore fluid pressure ratio, λ_i, from 0.2 to 0.4 (see additional models presented in the Supplementary Information). Future models will aim to incorporate these features.

In a final step, and to further explore how alteration can influence volcano stability, we modeled a scenario in which the highly altered zone identified by Rosas-Carbajal et al. (2016) was artificially enlarged to incorporate the entire southern flank (Figure 6d). Increasing the size of the alteration zone increases the surface velocities from ~0.05 to ~0.1 mm/yr and significantly increases the strain rate within the flank (Figure 6l). The slip surface that at the base of the deformable domain is now larger and has a higher strain rate, and the entire southern flank is now characterized by higher strain rates (Figure 6l). In addition, we also observe that expanding the alteration zone likely increases the potential collapse volume (Figure 6l). Based on these models, increasing the size of the highly altered zone (i.e. to a size larger than the present-day altered zone) will significantly increase the risk posed by the volcano. Deformation snapshots from additional models, presented in the Supplementary Information, show the progression of deformation for the present-day and increased-alteration scenarios from 5 to 100 kyrs (using upscaled physical and mechanical properties). These additional models also show that increasing the extent of the alteration increases the rate of volcano spreading.

5.4 Three-dimensional strength model for La Soufrière de Guadeloupe

The results of the previous section highlight the importance of combining geophysical surveys, laboratory data, and large-scale modeling to evaluate the influence of alteration on

volcanic flank instability. Our 2D model geometry is based on qualitative interpretations from an electrical conductivity model to delimit different regions based on their degree of alteration. A quantitative approach would require a petrophysical relation to convert the conductivity values to rock strength and cohesion, but such relations are highly non-unique as electrical conductivity depends on many factors including clay content, fluid temperature, and composition. Instead, rock strength is controlled to a first order by porosity, as shown in Figure 3b, and thus to the bulk rock density.

Here, we combine a 3D model of the bulk density of the present-day lava dome (Rosas-Carbajal et al., 2017) with an empirical power-law function relating wet bulk density and uniaxial compressive strength, σ_p, where $\sigma_p = 1.326^{-25}{\rho_w}^{9.67}$ (σ_p in Pa and ρ_w in kg/m^3) to create a 3D strength map of the volcano (Figure 7). The empirical function was specifically fitted to our new data for La Soufrière (Table 2; Figure 7a). Because the distribution of liquid-saturated and dry zones within the volcano is currently poorly constrained, we chose to use the bulk density of our samples saturated with liquid water, a scenario we consider better represents the natural state of the volcano than a completely dry volcano. The 3D bulk density model of Rosas-Carbajal et al. (2017) was obtained by jointly inverting gravity data and muon data acquired using three simultaneous muon detectors that scanned the lava dome from different points of view. Muon tomography is a novel technique, which uses the attenuation experienced by cosmic muons as they pass through the volcano to estimate its density (Tanaka et al., 2010). Whereas a single detector can provide 2D profiles of the average density of the volcano in the different directions sampled, multiple simultaneous detectors from different points of view can be used to create a 3D model of the volcano (Bonechi et al., 2020).

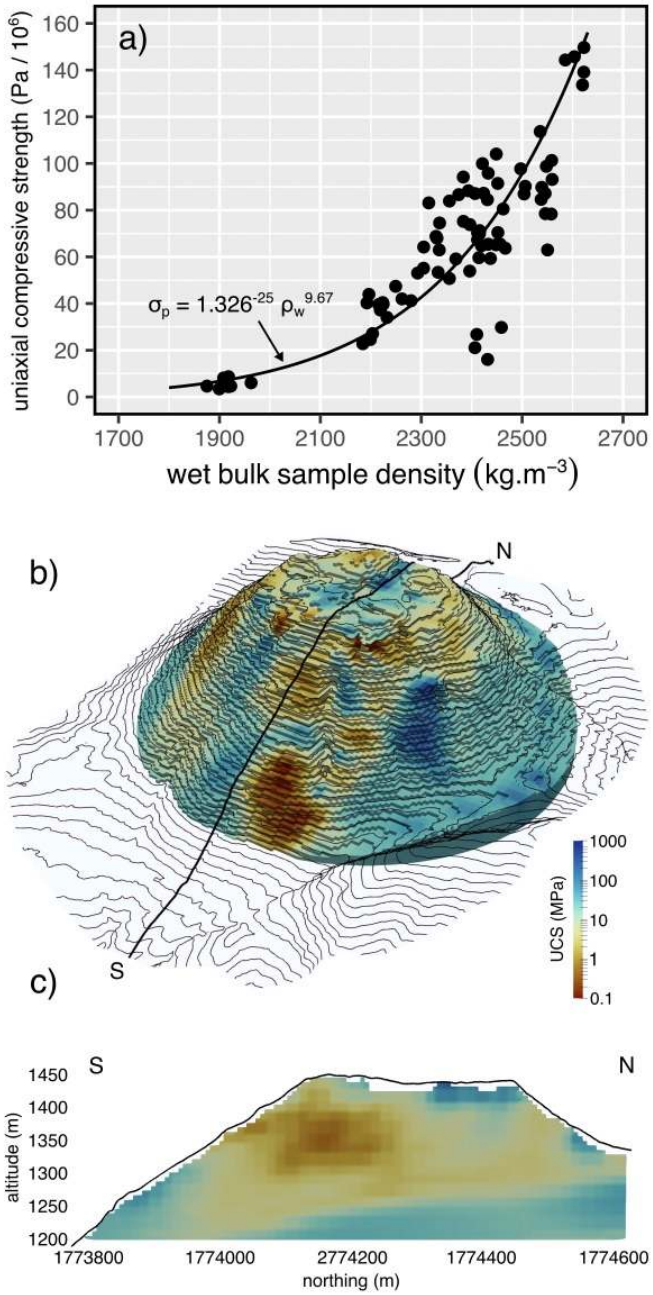

692

693 **Figure 7.** (a) Uniaxial compressive strength as a function of wet bulk sample density for
694 andesites from La Soufrière de Guadeloupe (Eastern Caribbean, France). Curve is the best-fit
695 empirical power-law function. (b) 3D uniaxial compressive strength map of La Soufrière de
696 Guadeloupe (Eastern Caribbean, France). The black line, which runs North-South, indicates
697 the position of the cross-section in panel (c). (c) North-South cross-section through La
698 Soufrière showing the distribution of uniaxial compressive strength. Color scale is the Roma

699 (seismic tomography) color scale of Fabio Crameri (Crameri et al., 2020). UCS – uniaxial
700 compressive strength.
701
702 Figure 7 highlights that large portions of the dome are characterized by very low values
703 of strength (< 5 MPa). In particular, the southern flank of the volcano hosts a significant weak
704 zone (Figures 7b and 7c). This low-strength zone is coincident with the location of the main
705 hydrothermal reservoir at La Soufrière, as exposed by electrical conductivity measurements
706 (Lesparre et al., 2012; Rosas-Carbajal et al., 2016). Based on (1) the influence of
707 hydrothermally altered rock on edifice stability and spreading rates at La Soufrière revealed by
708 the numerical modeling in the previous section, and (2) the large volume of low-strength rock
709 in the La Soufrière dome highlighted by our 3D strength model, we conclude that the stability
710 of La Soufrière is compromised by its high degree of rock alteration, and that the rate of volcano
711 spreading and the probability of an eventual partial edifice collapse may increase solely due to
712 the ongoing alteration caused by circulating hydrothermal fluids, and may not necessarily
713 require intensified hydrothermal and/or magmatic activity.
714 Based on our 3D strength model, we can provide estimates for the volumes of rock
715 within the lava dome below a certain strength threshold. For example, we estimate that rock
716 with a strength lower than 1 and 10 MPa comprises minimum dome volumes of 2.7×10^6 and
717 36×10^6 m^3, respectively, corresponding to at least 4% and 55% of the dome above 1200 m. In
718 other words, more than half of the La Soufrière dome could be considered to have a low
719 strength. We highlight that these volume and percentage estimates should be considered
720 conservative due to the positioning of the three telescopes at La Soufrière, which provides better
721 coverage of the southern flank of the volcano (Rosas-Carbajal et al., 2017). It is likely,
722 therefore, that the volumes and percentages of weak rock within the dome at La Soufrière are
723 higher than estimated here.

Although the strength map shown in Figure 7 is currently simplistic (for example, it is well known that strength increases with depth in the brittle field; Heap et al., 2015b; Figure 4), this 3D model permits the quick identification of zones within the volcano that could promote instability and more experimental data, when available, will allow us to account for depth and other factors that can influence rock mechanical behavior, such as temperature and saturation state (Heap and Violay, 2021).

6 Conclusions

Hydrothermal alteration is often invoked as a mechanism that greatly contributes to volcano instability (Reid et al., 2001; van Wyk de Vries et al., 2000). However, owing to the paucity of experimental data and the difficulty in accurately imaging subsurface alteration zones, the rock properties and the shape and size of the alteration zones required for large-scale modeling are often poorly constrained or even assumed. Here we use a combination of laboratory and geophysical data to numerically model the influence of hydrothermal alteration on volcano stability, using La Soufrière de Guadeloupe as a case study. Our numerical modeling suggests that hydrothermal alteration can significantly increase the deformation rate within the flanks of the volcano, and also increase the potential collapse volume.

The volcano stability modeling and 3D strength map presented herein, firsts for La Soufriere, help to validate the hypothesis forwarded by the numerous geophysical studies performed at the volcano: that the identified hydrothermal reservoir characterized by altered materials promotes volcano instability that could result in collapse (Bouligand et al., 2016; Brothelande et al., 2014; Lesparre et al., 2012; Nicollin et al., 2006; Rosas-Carbajal et al., 2016, 2017). As discussed above, eventual partial edifice collapse at La Soufrière may not necessarily require intensified hydrothermal and/or magmatic activity. Not only would the debris avalanche resulting from partial or major dome collapse threaten the inhabited areas surrounding the

749 volcano (Le Friant, 2006; Peruzzetto et al., 2019), but collapse could also depressurize the
750 hydrothermal system leading to steam-driven eruptions, dangerous laterally-directed
751 explosions, and associated high energy pyroclastic density currents, similar to the activity
752 during the 1976–1977 volcanic crisis (Feuillard et al., 1983; Komorowski et al., 2005). We also
753 highlight that the fragmentation threshold (the overpressure required for complete
754 fragmentation upon depressurization), the proportion of fines produced as a result of
755 fragmentation, and the ejection speed are also influenced by hydrothermal alteration (Mayer et
756 al., 2015, 2016; 2017; Montanaro et al., 2016), reinforcing the need for a multidisciplinary
757 approach to unravel how hydrothermal alteration affects volcanic hazards (see also de Moor et
758 al., 2019; Mick et al., 2021).

759 Our modeling and 3D strength map therefore highlight the importance of monitoring
760 the extent and evolution of hydrothermal alteration, and the formation of low-strength altered
761 layers, at La Soufrière and at other active volcanoes worldwide. Such monitoring can be
762 achieved, for example, using geophysical methods such as electrical tomography (Ahmed et
763 al., 2018; Byrdina et al., 2017; Ghorbani et al., 2018; Rosas-Carbajal et al., 2016) and muon
764 tomography (Lesparre et al., 2012; Rosas-Carbajal et al., 2017), near-surface seismic imaging
765 (Amoroso et al., 2018), thermal and gas monitoring (de Moor et al., 2019; Edmonds et al., 2003;
766 Jessop et al., 2021; Moretti et al., 2020; Tamburello et al., 2019), geological mapping (van Wyk
767 de Vries et al., 2000), deformation monitoring (Moretti et al., 2020), magnetic methods (Finn
768 et al., 2007), and remote and/or ground-based optical and spectroscopic methods (Crowley and
769 Zimbelman, 1997; Darmawan et al., 2018; John et al., 2008; Kereszturi et al., 2020; Mueller et
770 al., 2021). Further, although we document a reduction in strength as a function of alteration
771 (Figure 5c), alteration can also increase strength and potentially promote volcanic instability by
772 creating zones of high pore fluid pressure (Heap et al., 2021a; Reid, 2004). As noted in Heap
773 et al. (2021a), it is important not only to map the extent and evolution of hydrothermal

alteration, but also the locations in the volcano prone to porosity increasing and porosity decreasing alteration.

We have also shown that microtextural and mineralogical analysis of host-rock material erupted during phreatic explosive eruptions, as well as material from landslides and debris-avalanche deposits, can provide highly valuable insights into the nature, extent, and dynamics of alteration processes and fluid circulation in the pre-collapse edifice (see also Boudon et al., 1998; Komorowski et al., 2010; Salaün et al., 2011). Hence, we highlight that it is also important to quantify the mineral content of new material exposed by landslides and collapses, as well as their deposits, and to continuously monitor fluid compositions and water table fluctuations (Hurwitz et al., 2003) with respect to the geometry of weakened low-strength structures that are characteristic of the internal framework volcanic edifices hosting hydrothermal systems. A better understanding of the spatio-temporal evolution of hydrothermal alteration, and how it can influence volcano stability using large-scale modeling, will help improve the mitigation of volcanic hazards at active volcanoes worldwide.

Acknowledgements

This work was supported by the TelluS Program of INSU-CNRS ("Assessing the role of hydrothermal alteration on volcanic hazards") and ANR grant MYGALE ("Modelling the phYsical and chemical Gradients of hydrothermal ALteration for warning systems of flank collapse at Explosive volcanoes"), awarded to the first author. M. Heap also acknowledges support from the Institut Universitaire de France (IUF). We thank Tomaso Esposti Ongaro, Gilles Morvan, Christophe Nevado, Marie Cherrier, Océane Rocher, and Lisa Tomasetto. We thank the IPGP for general funding for the Observatoires Volcanologiques et Sismologiques (OVS), INSU-CNRS for the funding provided by the Service National d'Observation en Volcanologie (SNOV), and the Ministère pour la Transition Ecologique (MTE) for financial

799 support for the monitoring of the instable flank of La Soufrière de Guadeloupe. This study
800 contributes to the IdEx Université de Paris ANR-18-IDEX-0001. Olivier Roche, Jessica Ball,
801 and Gabor Kereszturi are thanked for providing comments that helped improve this manuscript.
802 All the mechanical data collected for this study can be downloaded here:
803 https://doi.org/10.6084/m9.figshare.14701137.v1.

804

805 **References**

806 Ahmed, A. S., Revil, A., Byrdina, S., Coperey, A., Gailler, L., Grobbe, N., ... & Hogg, C. (2018). 3D electrical
807 conductivity tomography of volcanoes. *Journal of Volcanology and Geothermal Research*, *356*, 243-263.
808 Amoroso, O., Festa, G., Bruno, P. P., D'Auria, L., De Landro, G., Di Fiore, V., ... & Zollo, A. (2018). Integrated
809 tomographic methods for seismic imaging and monitoring of volcanic caldera structures and geothermal
810 areas. Journal of Applied Geophysics, 156, 16-30.
811 Ball, J. L., Calder, E. S., Hubbard, B. E., & Bernstein, M. L. (2013). An assessment of hydrothermal alteration in
812 the Santiaguito lava dome complex, Guatemala: implications for dome collapse hazards. Bulletin of
813 Volcanology, 75(1), 1-18.
814 Ball, J. L., Stauffer, P. H., Calder, E. S., & Valentine, G. A. (2015). The hydrothermal alteration of cooling lava
815 domes. Bulletin of Volcanology, 77(12), 1-16.
816 Ball, J. L., Taron, J., Reid, M. E., Hurwitz, S., Finn, C., & Bedrosian, P. (2018). Combining multiphase
817 groundwater flow and slope stability models to assess stratovolcano flank collapse in the Cascade
818 Range. *Journal of Geophysical Research: Solid Earth*, *123*(4), 2787-2805.
819 Baumann, T. S., Kaus, B. J., & Popov, A. A. (2014). Constraining effective rheology through parallel joint
820 geodynamic inversion. Tectonophysics, 631, 197-211.
821 Baumann, T. S., & Kaus, B. J. (2015). Geodynamic inversion to constrain the non-linear rheology of the
822 lithosphere. *Geophysical Journal International*, *202*(2), 1289-1316.
823 Bauville, A., & Baumann, T. S. (2019). geomIO: An Open-Source MATLAB Toolbox to Create the Initial
824 Configuration of 2-D/3-D Thermo-Mechanical Simulations From 2-D Vector Drawings. *Geochemistry,*
825 *Geophysics, Geosystems*, *20*(3), 1665-1675.
826 Bonechi, L., D'Alessandro, R., & Giammanco, A. (2020). Atmospheric muons as an imaging tool. *Reviews in*
827 *Physics*, *5*, 100038.
828 Borgia, A., Delaney, P. T., & Denlinger, R. P. (2000). Spreading volcanoes. Annual Review of Earth and Planetary
829 Sciences, 28(1), 539-570.
830 Boudon, G., Semet, M. P., & Vincent, P. M. (1987). Magma and hydrothermally driven sector collapses: The 3100
831 and 11,500 y. BP eruptions of la Grande Decouverte (la Soufriere) volcano, Guadeloupe, French West
832 Indies. Journal of Volcanology and Geothermal Research, 33(4), 317-323.
833 Boudon, G., Villemant, B., Komorowski J.-C., Ildefonse, P., Semet, M.P. (1998) The hydrothermal system at
834 Soufriere Hills volcano, Montserrat (West Indies): Characterization and role in the ongoing eruption.
835 Geophysical Research Letters, 25: 3693-3696
836 Boudon, G., Komorowski, J.-C., Villemant, B., & Semet, M. P. (2008). A new scenario for the last magmatic
837 eruption of La Soufrière of Guadeloupe (Lesser Antilles) in 1530 AD Evidence from stratigraphy
838 radiocarbon dating and magmatic evolution of erupted products. Journal of Volcanology and Geothermal
839 Research, 178(3), 474-490.
840 Bouligand, C., Coutant, O., & Glen, J. M. (2016). Sub-surface structure of La Soufrière of Guadeloupe lava dome
841 deduced from a ground-based magnetic survey. Journal of Volcanology and Geothermal Research, 321,
842 171-181.
843 Brombach, T., Marini, L., & Hunziker, J. C. (2000). Geochemistry of the thermal springs and fumaroles of Basse-
844 Terre Island, Guadeloupe, Lesser Antilles. Bulletin of Volcanology, 61(7), 477-490.
845 Brothelande, E., Finizola, A., Peltier, A., Delcher, E., Komorowski, J. C., Di Gangi, F., ... & Legendre, Y. (2014).
846 Fluid circulation pattern inside La Soufrière volcano (Guadeloupe) inferred from combined electrical
847 resistivity tomography, self-potential, soil temperature and diffuse degassing measurements. Journal of
848 Volcanology and Geothermal Research, 288, 105-122.

Browne, P. R. L. (1978). Hydrothermal alteration in active geothermal fields. Annual Review of Earth and Planetary Sciences, 6, 229-250.

Byrdina, S., Friedel, S., Vandemeulebrouck, J., Budi-Santoso, A., Suryanto, W., Rizal, M. H., & Winata, E. (2017). Geophysical image of the hydrothermal system of Merapi volcano. *Journal of Volcanology and Geothermal Research*, *329*, 30-40.

Crameri, F., Shephard, G. E., & Heron, P. J. (2020). The misuse of colour in science communication. *Nature Communications*, *11*(1), 1-10.

Cecchi, E., van Wyk de Vries, B., & Lavest, J. M. (2004). Flank spreading and collapse of weak-cored volcanoes. *Bulletin of Volcanology*, *67*(1), 72-91.

Cole, P. D., Neri, A., & Baxter, P. J. (2015). Hazards from pyroclastic density currents. In *The Encyclopedia of Volcanoes* (pp. 943-956). Academic Press.

Crowley, J. K., & Zimbelman, D. R. (1997). Mapping hydrothermally altered rocks on Mount Rainier, Washington, with airborne visible/infrared imaging spectrometer (AVIRIS) data. *Geology*, *25*(6), 559-562.

Damby, D. E., Llewellin, E. W., Horwell, C. J., Williamson, B. J., Najorka, J., Cressey, G., & Carpenter, M. (2014). The α–β phase transition in volcanic cristobalite. Journal of Applied Crystallography, 47(4), 1205-1215.

Darmawan, H., Walter, T. R., Brotopuspito, K. S., & Nandaka, I. G. M. A. (2018). Morphological and structural changes at the Merapi lava dome monitored in 2012–15 using unmanned aerial vehicles (UAVs). Journal of Volcanology and Geothermal Research, 349, 256-267.

Day, S. J. (1996). Hydrothermal pore fluid pressure and the stability of porous, permeable volcanoes. *Geological Society, London, Special Publications*, *110*(1), 77-93.

de Moor, J. M., Stix, J., Avard, G., Muller, C., Corrales, E., Diaz, J. A., ... & Fischer, T. P. (2019). Insights on hydrothermal-magmatic interactions and eruptive processes at Poás Volcano (Costa Rica) from high-frequency gas monitoring and drone measurements. *Geophysical Research Letters*, *46*(3), 1293-1302.

del Potro, R., & Hürlimann, M. (2009). The decrease in the shear strength of volcanic materials with argillic hydrothermal alteration, insights from the summit region of Teide stratovolcano, Tenerife. *Engineering Geology*, *104*(1-2), 135-143.

Deyell, C. L., & Dipple, G. M. (2005). Equilibrium mineral–fluid calculations and their application to the solid solution between alunite and natroalunite in the El Indio–Pascua belt of Chile and Argentina. Chemical Geology, 215(1-4), 219-234.

Edmonds, M., Oppenheimer, C., Pyle, D. M., Herd, R. A., & Thompson, G. (2003). SO2 emissions from Soufrière Hills Volcano and their relationship to conduit permeability, hydrothermal interaction and degassing regime. Journal of Volcanology and Geothermal Research, 124(1-2), 23-43.

Ellis, A. J., & Mahon, W. A. J. (1977). Chemistry and geothermal systems (No. 553.79 E4).

Farquharson, J. I., Wild, B., Kushnir, A. R., Heap, M. J., Baud, P., & Kennedy, B. (2019). Acid-induced dissolution of andesite: evolution of permeability and strength. *Journal of Geophysical Research: Solid Earth*, *124*(1), 257-273.

Feuillard, M., Allegre, C. J., Brandeis, G., Gaulon, R., Le Mouel, J. L., Mercier, J. C., ... & Semet, M. P. (1983). The 1975–1977 crisis of La Soufrière de Guadeloupe (FWI): a still-born magmatic eruption. *Journal of Volcanology and Geothermal Research*, *16*(3-4), 317-334.

Feuillet, N., F. Beauducel, E. Jacques, P. Tapponnier, B. Delouis, S. Bazin, M. Vallée, and G. C. P. King (2011), The Mw = 6.3, November 21, 2004, Les Saintes earthquake (Guadeloupe): Tectonic setting, slip model and static stress changes, Journal of Geophysical Research, 116, B10301, doi:10.1029/2011JB008310.

Finn, C. A., Deszcz-Pan, M., Ball, J. L., Bloss, B. J., & Minsley, B. J. (2018). Three-dimensional geophysical mapping of shallow water saturated altered rocks at Mount Baker, Washington: Implications for slope stability. *Journal of Volcanology and Geothermal Research*, *357*, 261-275.

Frolova, J., Ladygin, V., Rychagov, S., & Zukhubaya, D. (2014). Effects of hydrothermal alterations on physical and mechanical properties of rocks in the Kuril–Kamchatka island arc. *Engineering Geology*, *183*, 80-95.

Ghorbani, A., Revil, A., Coperey, A., Ahmed, A. S., Roque, S., Heap, M. J., ... & Viveiros, F. (2018). Complex conductivity of volcanic rocks and the geophysical mapping of alteration in volcanoes. *Journal of Volcanology and Geothermal Research*, *357*, 106-127.

Girona, T., Realmuto, V., & Lundgren, P. (2021). Large-scale thermal unrest of volcanoes for years prior to eruption. Nature Geoscience, 14(4), 238-241.

Glicken, H. (1996). *Rockslide-debris avalanche of May 18, 1980, Mount St. Helens volcano, Washington* (No. 96-677). US Geological Survey.

Harlow, F. H., & Welch, J. E., 1965. Numerical calculation of time-dependent viscous incompressible flow of fluid with free surface. *The Physics of Fluids*, 8(12), 2182-2189.

Harnett, C. E., Kendrick, J. E., Lamur, A., Thomas, M. E., Stinton, A., Wallace, P. A., ... & Lavallée, Y. (2019). Evolution of mechanical properties of lava dome rocks across the 1995–2010 eruption of Soufrière Hills volcano, Montserrat. Frontiers in Earth Science, 7, 7.

Heap, M. J., Xu, T., & Chen, C.-f. (2014a). The influence of porosity and vesicle size on the brittle strength of volcanic rocks and magma. *Bulletin of Volcanology*, *76*(9), 856.

Heap, M. J., Lavallée, Y., Petrakova, L., Baud, P., Reuschlé, T., Varley, N. R., & Dingwell, D. B. (2014b). Microstructural controls on the physical and mechanical properties of edifice-forming andesites at Volcán de Colima, Mexico. Journal of Geophysical Research: Solid Earth, 119(4), 2925-2963.

Heap, M. J., Kennedy, B. M., Pernin, N., Jacquemard, L., Baud, P., Farquharson, J. I., ... & Dingwell, D. B. (2015a). Mechanical behaviour and failure modes in the Whakaari (White Island volcano) hydrothermal system, New Zealand. Journal of Volcanology and Geothermal Research, 295, 26-42.

Heap, M. J., Farquharson, J. I., Baud, P., Lavallée, Y., & Reuschlé, T. (2015b). Fracture and compaction of andesite in a volcanic edifice. *Bulletin of Volcanology*, *77*(6), 55.

Heap, M. J., Troll, V. R., Kushnir, A. R., Gilg, H. A., Collinson, A. S., Deegan, F. M., ... & Walter, T. R. (2019). Hydrothermal alteration of andesitic lava domes can lead to explosive volcanic behaviour. *Nature Communications*, *10*(1), 1-10.

Heap, M. J., Villeneuve, M., Albino, F., Farquharson, J. I., Brothelande, E., Amelung, F., ... & Baud, P. (2020a). Towards more realistic values of elastic moduli for volcano modelling. *Journal of Volcanology and Geothermal Research*, *390*, 106684.

Heap, M. J., Gravley, D. M., Kennedy, B. M., Gilg, H. A., Bertolett, E., & Barker, S. L. (2020b). Quantifying the role of hydrothermal alteration in creating geothermal and epithermal mineral resources: The Ohakuri ignimbrite (Taupō Volcanic Zone, New Zealand). *Journal of Volcanology and Geothermal Research*, *390*, 106703.

Heap, M. J., & Violay, M. E. (2021). The mechanical behaviour and failure modes of volcanic rocks: a review. Bulletin of Volcanology, 83(5), 1-47.

Heap M.J., Baumann, T., Gilg, H.A., Kolzenburg, S., Ryan, A., Villeneuve, M., Russell, J.K., Kennedy, L., Rosas-Carbajal, M., & Clynne M. (2021a) Hydrothermal alteration can result in pore pressurization and volcano instability. Geology, 49, https://doi.org/10.1130/G49063.1.

Heap, M. J., Wadsworth, F. B., Heng, Z., Xu, T., Griffiths, L., Velasco, A. A., ... & Deegan, F. M. (2021b). The tensile strength of volcanic rocks: Experiments and models. Journal of Volcanology and Geothermal Research, 107348.

Hemley, J. J., Hostetler, P. B., Gude, A. J., & Mountjoy, W. T. (1969). Some stability relations of alunite. *Economic Geology*, *64*(6), 599-612.

Henley, R. W., & Berger, B. R. (2011). Magmatic-vapor expansion and the formation of high-sulfidation gold deposits: Chemical controls on alteration and mineralization. Ore Geology Reviews, 39(1-2), 63-74.

Hincks, T. K., Komorowski, J. C., Sparks, S. R., & Aspinall, W. P. (2014). Retrospective analysis of uncertain eruption precursors at La Soufrière volcano, Guadeloupe, 1975–77: volcanic hazard assessment using a Bayesian Belief Network approach. *Journal of Applied Volcanology*, *3*(1), 3.

Hoek, E., & Diederichs, M. S. (2006). Empirical estimation of rock mass modulus. International journal of rock mechanics and mining sciences, 43(2), 203-215.

Horwell, C. J., Williamson, B. J., Llewellin, E. W., Damby, D. E., & Le Blond, J. S. (2013). The nature and formation of cristobalite at the Soufrière Hills volcano, Montserrat: implications for the petrology and stability of silicic lava domes. *Bulletin of Volcanology*, *75*(3), 696.

Hurwitz, S., Kipp, K. L., Ingebritsen, S. E., & Reid, M. E. (2003). Groundwater flow, heat transport, and water table position within volcanic edifices: Implications for volcanic processes in the Cascade Range. Journal of Geophysical Research: Solid Earth, 108(B12).

Inoue, A. (1995). Formation of clay minerals in hydrothermal environments. In: *Origin and mineralogy of clays* (pp. 268-329). Springer, Berlin, Heidelberg.

Jessop, D. E., Moune, S., Moretti, R., Gibert, D., Komorowski, J. C., Robert, V., ... & Burtin, A. (2021). A multi-decadal view of the heat and mass budget of a volcano in unrest: La Soufrière de Guadeloupe (French West Indies). Bulletin of Volcanology, 83(3), 1-19.

John, D. A., Sisson, T. W., Breit, G. N., Rye, R. O., & Vallance, J. W. (2008). Characteristics, extent and origin of hydrothermal alteration at Mount Rainier Volcano, Cascades Arc, USA: Implications for debris-flow hazards and mineral deposits. *Journal of Volcanology and Geothermal Research*, *175*(3), 289-314.

Karaman, K., & Kesimal, A. (2015). Evaluation of the influence of porosity on the engineering properties of volcanic rocks from the Eastern Black Sea Region: NE Turkey. Arabian Journal of Geosciences, 8(1), 557-564.

Kaus, B., Popov, A. A., Baumann, T., Pusok, A., Bauville, A., Fernandez, N., & Collignon, M. (2016). Forward and inverse modelling of lithospheric deformation on geological timescales. In: *Proceedings of NIC Symposium* (Eds: Binder, K., Müller, M., Kremer, M., Schnurpfeil, A.), John von Neumann Institute for Computing (NIC), NIC Series, Vol. 48, ISBN 978-3-95806-109-5.

Kennedy, B. M., Farquhar, A., Hilderman, R., Villeneuve, M. C., Heap, M. J., Mordensky, S., ... & Reuschlé, T. (2020). Pressure controlled permeability in a conduit filled with fractured hydrothermal breccia reconstructed from ballistics from Whakaari (White Island), New Zealand. Geosciences, 10(4), 138.

Kereszturi, G., Schaefer, L. N., Miller, C., & Mead, S. (2020). Hydrothermal Alteration on Composite Volcanoes: Mineralogy, Hyperspectral Imaging, and Aeromagnetic Study of Mt Ruapehu, New Zealand. *Geochemistry, Geophysics, Geosystems*, *21*(9), e2020GC009270.

Kereszturi, G., Schaefer, L., Mead, S., Miller, C., Procter, J., & Kennedy, B. (2021). Synthesis of hydrothermal alteration, rock mechanics and geophysical mapping to constrain failure and debris avalanche hazards at Mt. Ruapehu (New Zealand). New Zealand Journal of Geology and Geophysics, 1-22.

Kerle, N., & De Vries, B. V. W. (2001). The 1998 debris avalanche at Casita volcano, Nicaragua—investigation of structural deformation as the cause of slope instability using remote sensing. Journal of Volcanology and Geothermal Research, 105(1-2), 49-63.

Komorowski, J.-C., Boudon, G., Semet, M., Beauducel, F., Anténor-Habazac, C., Bazin, S., & Hammmouya, G. (2005). Guadeloupe. In: *Volcanic Atlas of the Lesser Antilles* (Eds: Lindsay, J., Robertson, R., Shepherd, J., & Ali, S.), University of the Fnrech West Indies, Seismic Research Unit, pp. 65-102.

Komorowski J-C., Legendre, Y., Christopher, T., Bernstein, L., R. Stewart, Joseph, E., Fournier, N., Chardot, L., Finizola, A., Wadge, G., Syers, R., Williams, C, Bass, V. (2010), Insights into processes and deposits of hazardous vulcanian explosions at Soufrière Hills Volcano during 2008 and 2009 (Montserrat, West Indies), Geophysical Research Letters, 37, L00E19, doi :10.1029/2010GL042558.

Komorowski, J.-C., Hincks, T., Sparks, R., Aspinall, W., & CASAVA ANR Project Consortium. (2015). Improving crisis decision-making at times of uncertain volcanic unrest (Guadeloupe, 1976). In: *Global Volcanic Hazards and Risk* (Eds: Loughlin, S.C., Sparks, R.S.J., Brown, S.K., Jenkins, S.F., & Vye-Brown, C), Cambridge University Press, pp 255-261.

Le Friant, A., Boudon, G., Komorowski, J. C., Heinrich, P., & Semet, M. P. (2006). Potential flank-collapse of Soufriere Volcano, Guadeloupe, lesser Antilles? Numerical simulation and hazards. *Natural Hazards*, *39*(3), 381.

Lesparre, N., Gibert, D., Marteau, J., Komorowski, J. C., Nicollin, F., & Coutant, O. (2012). Density muon radiography of La Soufriere of Guadeloupe volcano: comparison with geological, electrical resistivity and gravity data. Geophysical Journal International, 190(2), 1008-1019.

López, D. L., & Williams, S. N. (1993). Catastrophic volcanic collapse: relation to hydrothermal processes. *Science*, *260*(5115), 1794-1796.

Marini, L., Zuccolini, M. V., & Saldi, G. (2003). The bimodal pH distribution of volcanic lake waters. Journal of Volcanology and Geothermal Research, 121(1-2), 83-98.

Martel, C., Pichavant, M., Di Carlo, I., Champallier, R., Wille, G., Castro, J. M., ... & Kushnir, A. R. (2021). Experimental Constraints on the Crystallization of Silica Phases in Silicic Magmas. Journal of Petrology, 62(1), egab004.

Mayer, K., Scheu, B., Gilg, H. A., Heap, M. J., Kennedy, B. M., Lavallée, Y., ... & Dingwell, D. B. (2015). Experimental constraints on phreatic eruption processes at Whakaari (White Island volcano). Journal of Volcanology and Geothermal Research, 302, 150-162.

Mayer, K., Scheu, B., Montanaro, C., Yilmaz, T. I., Isaia, R., Aßbichler, D., & Dingwell, D. B. (2016). Hydrothermal alteration of surficial rocks at Solfatara (Campi Flegrei): Petrophysical properties and implications for phreatic eruption processes. Journal of Volcanology and Geothermal Research, 320, 128-143.

Mayer, K., Scheu, B., Yilmaz, T. I., Montanaro, C., Gilg, H. A., Rott, S., ... & Dingwell, D. B. (2017). Phreatic activity and hydrothermal alteration in the Valley of Desolation, Dominica, Lesser Antilles. Bulletin of Volcanology, 79(12), 82.

McCollom, T. M., Hynek, B. M., Rogers K., Moskowitz, B., & Berquó, T. S. (2013). Chemical and mineralogical trends during acid-sulfate alteration of pyroclastic basalt at Cerro Negro volcano and implications for early Mars. Journal of Geophysical Research, Planets, 118, 1719-1751.

Metcalfe, A., Moune, S., Komorowski, J. C., Kilgour, G., Jessop, D. E., Moretti, R., & Legendre, Y. (2021). Magmatic Processes at La Soufrière de Guadeloupe: Insights From Crystal Studies and Diffusion Timescales for Eruption Onset. Frontiers in Earth Science, 9, 78.

Meyer, C., & Hemley, J. J. (1967). Wall rock alteration in Barnes, HL (ed.) Geochemistry of hydrothermal ore deposits. Holt, Reinhart and Winston. Inc., New York.

Mick, E., Stix, J., de Moor, J. M., & Avard, G. (2021). Hydrothermal alteration and sealing at Turrialba volcano, Costa Rica, as a mechanism for phreatic eruption triggering. Journal of Volcanology and Geothermal Research, 107297.

Montanaro, C., Scheu, B., Mayer, K., Orsi, G., Moretti, R., Isaia, R., & Dingwell, D. B. (2016). Experimental investigations on the explosivity of steam-driven eruptions: A case study of Solfatara volcano (Campi Flegrei). Journal of Geophysical Research: Solid Earth, 121(11), 7996-8014.

Mordensky, S. P., Villeneuve, M. C., Kennedy, B. M., Heap, M. J., Gravley, D. M., Farquharson, J. I., & Reuschlé, T. (2018). Physical and mechanical property relationships of a shallow intrusion and volcanic host rock, Pinnacle Ridge, Mt. Ruapehu, New Zealand. *Journal of Volcanology and Geothermal Research*, *359*, 1-20.

Mordensky S., Heap M., Kennedy B., Gilg A., Villeneuve M., Farquharson J. and Gravley D. (2019) Influence of alteration on the mechanical behaviour and failure mode of andesite: implications for shallow seismicity and volcano monitoring. Bulletin of Volcanology, 81:44.

Moretti, R., Komorowski, J. C., Ucciani, G., Moune, S., Jessop, D., de Chabalier, J. B., ... & Deroussi, S. (2020). The 2018 unrest phase at La Soufrière of Guadeloupe (French West Indies) andesitic volcano: Scrutiny of a failed but prodromal phreatic eruption. *Journal of Volcanology and Geothermal Research*, *393*, 106769.

Mueller, D., Bredemeyer, S., Zorn, E., De Paolo, E., & Walter, T. R. (2021). Surveying fumarole sites and hydrothermal alteration by unoccupied aircraft systems (UAS) at the La Fossa cone, Vulcano Island (Italy). Journal of Volcanology and Geothermal Research, 413, 107208.

Nicolas, A., Lévy, L., Sissmann, O., Li, Z., Fortin, J., Gibert, B., & Sigmundsson, F. (2020). Influence of hydrothermal alteration on the elastic behaviour and failure of heat-treated andesite from Guadeloupe. *Geophysical Journal International*, *223*(3), 2038-2053.

Nicollin, F., Gibert, D., Beauducel, F., Boudon, G., & Komorowski, J. C. (2006). Electrical tomography of La Soufrière of Guadeloupe Volcano: Field experiments, 1D inversion and qualitative interpretation. Earth and Planetary Science Letters, 244(3-4), 709-724.

Opfergelt, S., Delmelle, P., Boivin, P., & Delvaux, B. (2006). The 1998 debris avalanche at Casita volcano, Nicaragua: Investigation of the role of hydrothermal smectite in promoting slope instability. Geophysical Research Letters, 33(15).

Peruzzetto, M., Komorowski, J.-C., Le Friant, A., Rosas-Carbajal, M., Mangeney, A., & Legendre, Y. (2019). Modeling of partial dome collapse of La Soufrière of Guadeloupe volcano: implications for hazard assessment and monitoring. *Scientific Reports*, *9*(1), 1-15.

Pusok, A. E., & Kaus, B. J. (2015). Development of topography in 3-D continental-collision models. *Geochemistry, Geophysics, Geosystems*, *16*(5), 1378-1400.

Reid, M. E., Sisson, T. W., & Brien, D. L. (2001). Volcano collapse promoted by hydrothermal alteration and edifice shape, Mount Rainier, Washington. *Geology*, *29*(9), 779-782.

Reid, M. E. (2004). Massive collapse of volcano edifices triggered by hydrothermal pressurization. *Geology*, *32*(5), 373-376.

Reuber, G. S., Kaus, B. J., Popov, A. A., & Baumann, T. S. (2018). Unraveling the physics of the Yellowstone magmatic system using geodynamic simulations. Frontiers in Earth Science, 6, 117.

Rosas-Carbajal, M., Komorowski, J. C., Nicollin, F., & Gibert, D. (2016). Volcano electrical tomography unveils edifice collapse hazard linked to hydrothermal system structure and dynamics. *Scientific reports*, *6*, 29899.

Rosas-Carbajal, M., Jourde, K., Marteau, J., Deroussi, S., Komorowski, J. C., & Gibert, D. (2017). Three-dimensional density structure of La Soufrière de Guadeloupe lava dome from simultaneous muon radiographies and gravity data. *Geophysical Research Letters*, *44*(13), 6743-6751.

Roverato, M., Di Traglia, F., Procter, J., Paguican, E., & Dufresne, A. (2021). Factors contributing to volcano lateral collapse. In Volcanic Debris Avalanches (pp. 91-119). Springer, Cham.

Rye, R. O., Bethke, P. M., & Wasserman, M. D. (1992). The stable isotope geochemistry of acid sulfate alteration. Economic Geology, 87(2), 225-262.

Salaün, A., Villemant, B., Gérard, M., Komorowski, J. C., & Michel, A. (2011). Hydrothermal alteration in andesitic volcanoes: trace element redistribution in active and ancient hydrothermal systems of Guadeloupe (Lesser Antilles). *Journal of Geochemical Exploration*, *111*(3), 59-83.

Samaniego, P., Valderrama, P., Mariño, J., van Wyk de Vries, B., Roche, O., Manrique, N., ... & Malnati, J. (2015). The historical (218±14 aBP) explosive eruption of Tutupaca volcano (Southern Peru). Bulletin of Volcanology, 77(6), 1-18.

Schaefer, L. N., Kendrick, J. E., Oommen, T., Lavallée, Y., & Chigna, G. (2015). Geomechanical rock properties of a basaltic volcano. *Frontiers in Earth Science*, *3*, 29.

Schipper, C. I., Rickard, W. D., Reddy, S. M., Saxey, D. W., Castro, J. M., Fougerouse, D., ... & Lilly, K. (2020). Volcanic SiO2-cristobalite: A natural product of chemical vapor deposition. *American Mineralogist: Journal of Earth and Planetary Materials*, *105*(4), 510-524.

Siebert, L. (1984) Large volcanic debris avalanches: characteristics of source areas, deposits, and associated eruptions. Journal of Volcanology and Geothermal Research 22, 163–197.

Siebert, L., Glicken, H. & Ui, T. (1987). Volcanic hazards from Bezymianny- and Bandai-type eruptions. Bulletin of Volcanology 49, 435–459.

Siebert, L., Simkin, T. & Kimberly, P. Volcanoes of the World (Univ of California Press, 2010).

Siratovich, P. A., Heap, M. J., Villenueve, M. C., Cole, J. W., & Reuschlé, T. (2014). Physical property relationships of the Rotokawa Andesite, a significant geothermal reservoir rock in the Taupo Volcanic Zone, New Zealand. Geothermal Energy, 2(1), 1-31.

Sparks, R.S.J., Barclay, J., Calder, E.S., Herd, R.A., Komorowski, J-C., Norton, G.E., Ritchie, L., Voight, B., Woods, A.W. (2002) Generation of a debris avalanche and violent pyroclastic density current: the Boxing Day eruption of 26 December 1997 at the Soufrière Hills Volcano, Montserrat. In: T.H. Druitt, B.P. Kokelaar (Eds), The eruption of Soufrière Hills Volcano, Montserrat, from 1995 to 1999, Geological Society, London, Memoirs, 21, 409-43

Stoffregen, R. E., & Cygan, G. L. (1990). An experimental study of Na-K exchange between alunite and aqueous sulfate solutions. American Mineralogist, 75(1-2), 209-220.

Stoffregen, R. E., Alpers, C. N., & Jambor, J. L. (2000). Alunite-jarosite crystallography, thermodynamics, and geochronology. Reviews in Mineralogy and Geochemistry, 40(1), 453-479.

Tamburello, G., Moune, S., Allard, P., Venugopal, S., Robert, V., Rosas-Carbajal, M., ... & Moretti, R. (2019). Spatio-temporal relationships between fumarolic activity, hydrothermal fluid circulation and geophysical signals at an arc volcano in degassing unrest: La Soufrière of Guadeloupe (French West Indies). Geosciences, 9(11), 480.

Tanaka, H. K., Taira, H., Uchida, T., Tanaka, M., Takeo, M., Ohminato, T., ... & Tsuiji, H. (2010). Three-dimensional computational axial tomography scan of a volcano with cosmic ray muon radiography. *Journal of Geophysical Research: Solid Earth*, *115*(B12).

Taran, Y., & Kalacheva, E. (2020). Acid sulfate-chloride volcanic waters; Formation and potential for monitoring of volcanic activity. Journal of Volcanology and Geothermal Research, 107036.

van Wyk de Vries, B., & Francis, P. W. (1997). Catastrophic collapse at stratovolcanoes induced by gradual volcano spreading. *Nature*, *387*(6631), 387-390.

van Wyk de Vries, B., Kerle, N., & Petley, D. (2000). Sector collapse forming at Casita volcano, Nicaragua. *Geology*, *28*(2), 167-170.

Vásárhelyi, B. (2009). A possible method for estimating the Poisson's rate values of the rock masses. Acta Geodaetica et Geophysica Hungarica, 44(3), 313-322.

Villemant, B, Hammouya, G, Michel, A., Semet, M., Komorowski J-C, Boudon, G., Cheminée, J-L. (2005) The memory of volcanic waters: shallow magma degassing revealed by halogen monitoring in thermal springs of La Soufrière volcano (Guadeloupe, Lesser Antilles), Earth Planet. Sci. Letters, 237: 710-728.

Villemant, B., Komorowski, J. C., Dessert, C., Michel, A., Crispi, O., Hammouya, G., ... & De Chabalier, J. B. (2014). Evidence for a new shallow magma intrusion at La Soufrière of Guadeloupe (Lesser Antilles): insights from long-term geochemical monitoring of halogen-rich hydrothermal fluids. Journal of Volcanology and Geothermal Research, 285, 247-277.

Voight B., Glicken, H., Janda, R.J., Douglass, P.M. (1981) Catastrophic rockslide avalanche of May 18. In: Lipman, P. W. & Mullineaux, D. R. (Eds) The 1980 Eruptions of Mount St Helens, Washington, US Geological Survey, Professional Papers, 1250, 347-378.

Voight, B., Komorowski J-C., Norton, G.E., Belousov, A.B., Belousova, M., Boudon, G., Francis, P.W., Franz, W., Heinrich, P., Sparks, R.S.J. & Young, S.R. (2002) The 1997 Boxing Day Sector Collapse and Debris Avalanche, Soufriere Hills Volcano, Montserrat, W.I. In: T.H. Druitt, B.P. Kokelaar (Eds), The eruption of Soufrière Hills Volcano, Montserrat, from 1995 to 1999, Geological Society, London Memoirs, 21, 363-407

Watters, R. J., & Delahaut, W. D. (1995). Effect of argillic alteration on rock mass stability. Clay and Shale Slope Instability, 10, 139.

Watters, R. J., Zimbelman, D. R., Bowman, S. D., & Crowley, J. K. (2000). Rock mass strength assessment and significance to edifice stability, Mount Rainier and Mount Hood, Cascade Range volcanoes. *Pure and Applied Geophysics*, *157*(6-8), 957-976.

Wyering, L. D., Villeneuve, M. C., Wallis, I. C., Siratovich, P. A., Kennedy, B. M., Gravley, D. M., & Cant, J. L. (2014). Mechanical and physical properties of hydrothermally altered rocks, Taupo Volcanic Zone, New Zealand. *Journal of Volcanology and Geothermal Research*, *288*, 76-93.

Yilmaz, T. I., Wadsworth, F. B., Gilg, H. A., Hess, K. U., Kendrick, J. E., Wallace, P. A., ... & Dingwell, D. B. (2021). Rapid alteration of fractured volcanic conduits beneath Mt Unzen. Bulletin of Volcanology, 83(5), 1-14.

Zhu, W., Baud, P., Vinciguerra, S., & Wong, T. F. (2016). Micromechanics of brittle faulting and cataclastic flow in Mount Etna basalt. Journal of Geophysical Research: Solid Earth, 121(6), 4268-4289.

Zimbelman, D. R., Rye, R. O., & Breit, G. N. (2005). Origin of secondary sulfate minerals on active andesitic stratovolcanoes. Chemical Geology, 215(1-4), 37-60.